

**MODAL ANALYSIS OF AEROFOIL CROSS-SECTIONED WING MADE OF LAMINATED COMPOSITE AND FILLED WITH FOAM**

**A Thesis Submitted to  
the Graduate School of Engineering and Sciences of  
İzmir Institute of Technology  
in Partial Fulfillment of the Requirements for the Degree of**

**MASTER OF SCIENCE**

**in Mechanical Engineering**

**by  
Barış İSKEÇE**

**October 2015  
İZMİR**

We approve the thesis of **Barış İSKEÇE**

**Examining Committee Members:**

---

**Prof. Dr. Bülent YARDIMOĞLU**

Department of Mechanical Engineering, İzmir Institute of Technology

---

**Assist. Prof. Dr. Onursal ÖNEN**

Department of Mechanical Engineering, İzmir Institute of Technology

---

**Assoc. Prof. Dr. Levent MALGACA**

Department of Mechanical Engineering, Dokuz Eylül University

**23 October 2015**

---

**Prof. Dr. Bülent YARDIMOĞLU**

Supervisor, Department of Mechanical Engineering,  
İzmir Institute of Technology

---

**Prof. Dr. Metin TANOĞLU**

Head of the Department of  
Mechanical Engineering

---

**Prof. Dr. R. Bilge KARAÇALI**

Dean of the Graduate School  
of Engineering and Sciences

## ACKNOWLEDGEMENTS

A number of people deserve thanks for their support and help. It is therefore my greatest pleasure to express my gratitude to them all in this acknowledgement.

The author wishes to express his gratitude to his supervisors, Professor Dr. Bülent YARDIMOĞLU who was abundantly helpful and offered invaluable assistance, support and guidance.

Special thanks also to all friends, especially group members; Melih AKGÜNEYLI and Çetin Özgür BALTAÇI for sharing the literature and invaluable assistance.

Furthermore, I would like to acknowledge the help I received from Ercüment ALYANAK, ENA YELKAPAN TEKNOLOJİLERİ. I have benefited from their design parameters.

The author wishes to express her love and gratitude to her beloved families; for their understanding & endless love, through the duration of his studies.

Finally, to my caring, loving, and supportive wife, Ayşegül: my deepest gratitude. Her support, encouragement, quiet patience and unwavering love were undeniably. She has been my inspiration and motivation for continuing to improve my knowledge and move my career forward.

I dedicate this thesis to my wife Ayşegül and to my daughter.

## **ABSTRACT**

### **MODAL ANALYSIS OF AEROFOIL CROSS-SECTIONED WING MADE OF LAMINATED COMPOSITE AND FILLED WITH FOAM**

Modal analysis of aerofoil cross-sectioned wing made of laminated composite and filled with foam is studied by Finite Element Method with the help of ANSYS which is very powerful and well proven software all around the world. The effects of ratio of overhangs to mid-span and length of the thickened parts on natural frequencies are investigated by finite element models developed in ANSYS and the model is verified by theoretical results available in the literature.

## ÖZET

### KÖPÜKLE DOLDURULMUŞ VE TABAKALI KOMPOZİTTEN YAPILMIŞ AEROFOİL KESİTLİ KANADIN MODAL ANALİZİ

Köpükle doldurulmuş ve tabakalı kompozitten yapılmış aerofoil kesitli kanadın modal analizi, Dünya’da iyi ispatlanmış ve güçlü bir sonlu eleman yazılımı olan ANSYS’in yardımı ile çalışılmıştır. Çıkıntının açıklığa oranının ve takviyelenmiş kısımların uzunluklarının doğal frekanslara etkileri ANSYS de geliştirilen sonlu eleman modelleri ile araştırılmıştır ve model kaynaklarda mevcut sonuçlar ile karşılaştırılarak doğrulanmıştır.

# TABLE OF CONTENTS

LIST OF FIGURES .....	vii
LIST OF TABLES .....	viii
LIST OF SYMBOLS .....	ix
CHAPTER 1. GENERAL INTRODUCTION .....	1
CHAPTER 2. THEORETICAL BACKGROUND .....	9
2.1. Description of the Problem .....	9
2.2. Modal Analysis of Multi-Part Wing .....	11
2.3. Vibration of Simply Supported Beams with Overhang .....	13
2.4. Mechanics of Laminated Composites.....	16
2.4.1. Macromechanical Analysis of a Lamina .....	16
2.4.2. Macromechanical Analysis of Laminates.....	18
2.4.3. Material Properties of Cross-Section of the Wing.....	22
2.5. Modal Analysis by Finite Element Method.....	23
CHAPTER 3. NUMERICAL RESULTS AND DISCUSSION.....	25
3.1. Geometrical Model of the Wing .....	25
3.2. Material Models of the Wing.....	28
3.3. Verification of the Present Model.....	30
3.4. Natural Frequencies and Mode Shapes of Main Model .....	33
3.5. Natural Frequencies and Mode Shapes of Several Models .....	39
CHAPTER 4. CONCLUSIONS .....	47
REFERENCES .....	48

## LIST OF FIGURES

<u>Figure</u>	<u>Page</u>
Figure 1.1. Fiber composite .....	4
Figure 1.2. Particulate composite .....	4
Figure 1.3. Flake composite.....	4
Figure 1.4. Filled composite .....	4
Figure 1.5. Laminar composite .....	5
Figure 1.6. Various composite materials used in structures of the Boeing 777 .....	6
Figure 2.1. A wing with two overhangs.....	9
Figure 2.2. Cross-section of the wing .....	10
Figure 2.3. Geometry of simply supported beam with symmetric overhang .....	13
Figure 2.4 Transformed fundamental root of the frequency equation for a simply supported beam with symmetric overhang .....	15
Figure 2.5. Local and global axes of an angle lamina. ....	16
Figure 2.6. Schematic of a laminate .....	18
Figure 2.7. Resultant forces and moments on a laminate .....	19
Figure 2.8. Coordinate locations of plies in a laminate. ....	20
Figure 2.9. Parts of the cross-section of the wing in x-y plane.....	22
Figure 2.10: Flapping lead-lag and torsional motions of a rotating beam.....	24
Figure 3.1. Dimensions of the wing with two equal overhangs .....	25
Figure 3.2. Cross-section of the wing with part numbers.....	25
Figure 3.3. Dimensions of the uniform wing with two equal overhangs.....	30
Figure 3.4. Covergency curve.....	31
Figure 3.5. First natural mode shape: Flapping 1 .....	32
Figure 3.6. Second natural mode shape: Flapping .....	32
Figure 3.7. Third natural mode shape: Flapping 3 .....	33
Figure 3.8. Dimensions of the wing with two equal overhangs .....	33
Figure 3.9. Flapping 1 .....	34
Figure 3.10. Flapping 2 .....	35
Figure 3.11. Flapping 3 .....	35
Figure 3.12. Lead-Lag 1. ....	36
Figure 3.13. Flapping 4.....	36

Figure 3.14. Lead-Lag 2 .....	37
Figure 3.15. Lead-Lag 3 .....	37
Figure 3.16. Flapping 5 .....	38
Figure 3.17. Flapping 6 .....	38
Figure 3.18. Flapping 7 .....	39
Figure 3.19. The effect of L1 on first natural frequencies .....	40
Figure 3.20. The effect of L1 on second natural frequencies .....	41
Figure 3.21. The effect of L1 on third natural frequencies .....	41
Figure 3.22. The effect of L1 on fourth natural frequencies .....	41
Figure 3.23. The effect of L1 on fifth natural frequencies .....	42
Figure 3.24. The effect of L1 on sixth natural frequencies .....	42
Figure 3.25. The effect of L1 on seventh natural frequencies .....	42
Figure 3.26. The effect of L1 on eighth natural frequencies .....	43
Figure 3.27. The effect of L1 on ninth natural frequencies .....	43
Figure 3.28. The effect of L1 on tenth natural frequencies .....	43
Figure 3.29. The effect of L2 on first natural frequencies .....	45
Figure 3.30. The effect of L2 on second natural frequencies .....	45
Figure 3.31. The effect of L2 on third natural frequencies .....	45



## LIST OF TABLES

<b><u>Table</u></b>	<b><u>Page</u></b>
Table 3.1 Geometrical properties of each part for <i>thickness of Part 1</i> = 3.2 mm.....	26
Table 3.2 Geometrical properties of each part for <i>thickness of Part 1</i> = 5 mm.....	26
Table 3.3 Laminate codes and layer thicknesses for C-S1 .....	28
Table 3.4 Laminate codes and layer thicknesses for C-S2 .....	28
Table 3.5 Axial and shear modulus .....	29
Table 3.6 Eqv (equivalent) densities and axial Young's modulus .....	30
Table 3.7 Comparisons of natural frequencies (Hz).....	31
Table 3.8. Natural frequencies $f_i$ (Hz) with N=40 elements.....	34

## LIST OF SYMBOLS

$E_1$	Longitudinal elastic modulus
$E_2$	Transverse elastic modulus
$f$	natural frequency
$G_{12}$	Shear modulus
$\nu_{12}$	Major Poisson's ratio
$\rho$	density (kg/m <sup>3</sup> )
$\sigma_{1 \text{ ult}}^T$	Ultimate longitudinal tensile strength
$\sigma_{1 \text{ ult}}^C$	Ultimate longitudinal compressive strength
$\sigma_{2 \text{ ult}}^T$	Ultimate transverse tensile strength
$\sigma_{2 \text{ ult}}^C$	Ultimate transverse compressive strength
$\tau_{12}$	Ultimate in-plane shear strength
( $\dot{\quad}$ )	differentiation with respect to time

# CHAPTER 1

## GENERAL INTRODUCTION

The word composite in the term composite material signifies that two or more materials are combined on a macroscopic scale to form a useful third material. The key is the macroscopic examination of a material wherein the components can be identified by the naked eye. Different materials can be combined on a microscopic scale, such as in alloying of metals, but the resulting material is, for all practical purposes, macroscopically homogeneous, i.e., the components cannot be distinguished by the naked eye and essentially act together. The advantage of composite materials is that, if well designed, they usually exhibit the best qualities of their components or constituents and often some qualities that neither constituent possesses. Some of the properties that can be improved by forming a composite material are (Jones, 1999)

- strength
- stiffness
- corrosion resistance
- wear resistance
- attractiveness
- weight
- fatigue life
- temperature-dependent behavior
- thermal insulation
- thermal conductivity
- acoustical insulation

Naturally, not all of these properties are improved at the same time nor is there usually any requirement to do so. In fact, some of the properties are in conflict with one another, e.g., thermal insulation versus thermal conductivity. The objective is merely to create a material that has only the characteristics needed to perform the design task (Jones, 1999).

Throughout history, humans have used composite type materials. One of the earliest uses of composite material was by the ancient Mesopotamians around 3400 B.C., when they glued wood strips at different angles to create plywood.

Egyptians used of Cartonnage, layers of linen or papyrus soaked in plaster, for death masks dates to the 2181-2055 BC. Archeologists have found that natural composite building materials were in used in Egypt and Mesopotamia, since ancient builders and artisans used straw to reinforce mud bricks, pottery, and boats around 1500 BC.

Around 25 BC, The Ten Books on Architecture described concrete and distinguished various types of lime and mortars. Researchers have demonstrated that the cement described in the books is similar, and in some ways superior to the Portland cement used today.

In about 1200 AD, the Mongols invented the first composite bows made from a combination of wood, bamboo, bone, cattle tendons, horns, bamboo and silk bonded with natural pine resin. The bows were small, very powerful, and extremely accurate. Composite Mongolian bows were the most feared weapons on earth until the invention effective firearms in the 14th century.

Chemistry had revolution about the 1880. Polymerization allowed new synthetic resins to be transformed from a liquid to solid state in a cross-linked molecular structure. Early synthetic resins included celluloid, melamine and Bakelite.

In the early 1900's, plastics such as vinyl, polystyrene, phenolic and polyester were developed. As important as these innovations were, reinforcement was needed to provide the strength and rigidity.

Bakelite, or polyoxybenzylmethylenglycolanhydride, is an early innovative plastic. It is a thermosetting phenol formaldehyde resin, formed from an elimination reaction of phenol with formaldehyde. It was developed by Belgian-born chemist Leo Baekeland in New York in 1907.

One of the first plastics made from synthetic components, Bakelite was used for its electrical nonconductivity and heat-resistant properties in electrical insulators, radio and telephone casings, and such diverse products as kitchenware, jewelry, pipe stems, and children's toys. Bakelite was designated a National Historic Chemical Landmark in 1993 by the American Chemical Society in recognition of its significance as the world's first synthetic plastic. The "retro" appeal of old Bakelite products has made them collectible.

The thirties were perhaps the most important decade for the composites industry. In 1935, Owens Corning launched the fiber reinforce polymer (FRP) industry by introducing

the first glass fiber. In 1936, unsaturated polyester resins were patented. Because of their curing properties, they would become the dominant choice for resins in manufacturing today. In 1938, other higher performance resin systems like epoxies also became available.

World War II brought the FRP industry from research into actual production. In addition to high strength to weight properties, fiberglass composites were found to be transparent to radio frequencies and were adopted for radar domes and used with other electronic equipment. In addition, the war effort developed first commercial grade boat hulls. While they were not deployed in the war effort, the technology was rapidly commercialized after the war.

By 1947 a fully composite body automobile had been made and tested. This car was reasonably successful and led to the development of the 1953 Corvette, which was made using fiberglass preforms impregnated with resin and molded in matched metal dies. During this period, several methods for molding were developed. Eventually two methods, compression molding of sheet molding compound (SMC) and bulk molding compound (BMC), would emerge as the dominant forms of molding for the automotive and other industries.

In early 1950's, manufacturing methods such included pultrusion, vacuum bag molding, and large-scale filament winding were developed. Filament winding became the basis for the large-scale rocket motors that propelled exploration of space in the 1960's and beyond. Pultrusion is used today in the manufacture of linear components such as ladders and moldings.

In 1961, first carbon fiber was patented, but it was several years before carbon fiber composites were commercially available. Carbon fibers improved thermoset part stiffness to weight ratios, thereby opening even more applications in aerospace, automotive, sporting goods, and consumer goods. The marine market was the largest consumer of composite materials in the 1960's.

By the mid 1990's, composites hit mainstream manufacturing and construction. As a cost effective replacement to traditional materials like metal and engineered thermoplastics, Engineers began specifying thermoset composites for various components within the Appliance, Construction, Electrical and Transportation industries (<http://www.mar-bal.com/applications/history-of-composites/>).

Classification of composite materials are given by Vinson ( 2002) as:

- Fiber: Either continuous (long or chopped whiskers) are suspended in a matrix material shown in Figure 1.1.
- Particulate: Composed of particles are suspended in a matrix material (Figure 1.2).
- Flake: Composed of flakes which have large ratios of platform area to thickness and are suspended in a matrix material (Figure 1.3)
- Filled/Skeletal: Composed of a continuous skeletal matrix filled by a second material (Figure 1.4)
- Laminar: Composed of layers bonded together by a matrix material (Figure 1.5).

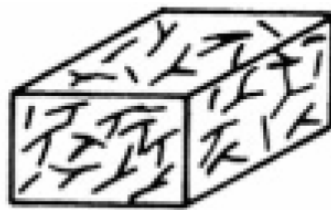


Figure 1.1. Fiber composite  
(Source: Vinson 2002)

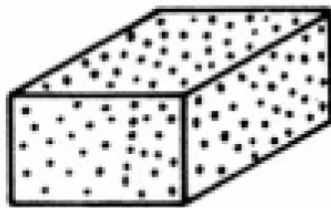


Figure 1.2. Particulate composite  
(Source: Vinson 2002)

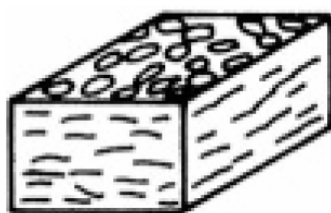


Figure 1.3. Flake composite  
(Source: Vinson 2002)



Figure 1.4. Filled composite  
(Source: Vinson 2002)

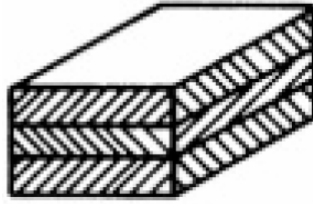


Figure 1.5. Laminar composite  
(Source: Vinson 2002)

Composites are different from metals and are combinations of materials differing in composition or form. The constituents retain their identities in the composites, and do not dissolve or otherwise merge completely into each other, although they act together. Reinforced concrete is an excellent example of a composite structure in which the concrete and steel still retain their identities. The steel bars carry the tension loads, and the concrete carries the compression loads. In aircraft construction, the term composite structures refers to fabric resin combinations in which the fabric is embedded in the resin, but still retains its identity.

Advanced composite materials consist of new high strength fibers embedded in an epoxy matrix. These composites provide for major weight savings in airplane structures, since they have high strength to weight ratios. When replacing aluminum structure with graphite/epoxy composite, weight reductions of 20% or better are possible. Weight reduction is the greatest advantage of composite material, and is one of the key items in decisions regarding its selection. Other advantages over conventional structure include, its high corrosion resistance, and its resistance to damage from cyclic loading (fatigue).

The major disadvantage of using advanced composite materials in airplane construction is the relatively high cost of the materials.

Hybrid Composites are made by the addition of some complementary material such as fiberglass or kevlar to the basic carbon fiber/epoxy matrix. The added materials are used to obtain specific material characteristics, such as greater fracture toughness and impact resistance, and should be considered for areas subject to foreign object damage. The addition of carbon / epoxy to fiberglass structure is used to provide additional stiffness (<http://www.aviation-history.com/theory/composite.htm>).

Figure 1.6 shows the application of various composite materials on the Boeing 777.

For rotor blades, composite materials provide opportunities for structural simplicity of hingeless and bearingless designs, increased fatigue life, and structural couplings to improve the response and the aeroelastic stability of configurations. The directional nature

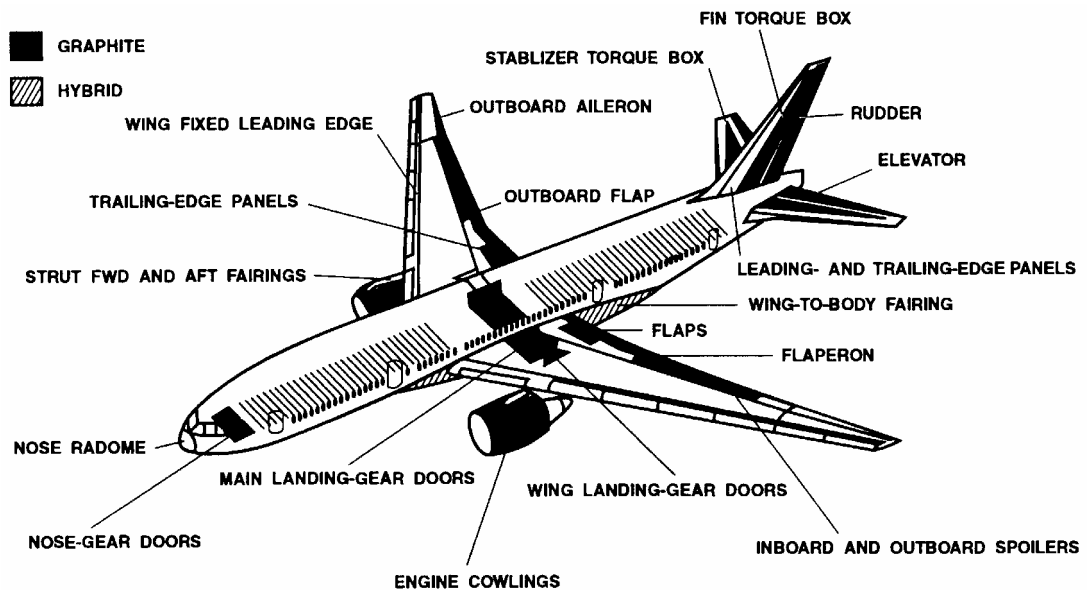


Figure 1.6 Various composite materials used in structures of the Boeing 777  
(Source: Jones 1999)

of the composite materials allows for construction of rotor blades with different ply orientations of materials exhibiting coupling between the elastic modes of deformation. Plies with an appropriate placement of fibers in the blade can produce elastic coupling between desired types of motion in the modes, thus providing a mechanism for elastic tailoring.

Since rotor blades are built-up, complicated structures, some simplification in the analytical modeling is helpful in the process of designing them and studying their behavior. One such simplification is to regard the blade as a beam. For analysis of composite rotor blades as beams, it is necessary to determine a constitutive law that is suitable for beam theory.

Composite materials are commonly used in industry because of their low weight, high strength, precise shape. Glass fiber or carbon fiber with epoxy are main materials for composite structures. Composite materials also exhibit desired damping properties due to their structural properties such as lamination or combinations. The energy dissipation for damping is based on the resin (generally epoxy).



The first of beam theory has been introduced by Euler (1744). After this, the most popular one has been introduced by Timoshenko (1744). Several textbooks have been written for the Mechanics of Composite Materials ( Tsai, 1980; Jones, 1999; Vinson, 2002; Kaw, 2006). Recently, Qatu (2004) published a textbook on vibration of laminated shells and plates.

Stafford and Giurgiutiu (1975) presented an important study on semi-analytic methods for rotating Timoshenko beams.

Jang and Bert (1989) derived the frequency equations for vibrating stepped beams on classical supports.

Murphy (1997) found the numerical solution to the frequency equation for the transverse vibration of a simple beam with symmetric overhangs.

Hodges et al (1989) presented the natural frequencies and mode shapes of composite beam structures. The sectional elastic constants are determined from two qualitatively different methods: simple analytical methods in which the stiffnesses are given in closed form and a detailed cross-sectional finite element method. The equations of motion are also solved in two ways: by an essentially exact integration method and by a mixed finite element method.

Subic and He (1995) presented a modal parameter estimation methods to the analysis of a high performance glider wing. Due to the aerodynamic characteristics of the glider wing, material and design characteristics of laminated composite structure, experimental modal analysis is different from the case of powered aircraft analysis. Damping factors of the overall structure is particularly interesting in this case study.

Marur and Kant (1996) studied on free vibration analysis of fiber reinforced composite beams using higher order theories and finite element modelling. They used Taylor's series expansions for axial displacement in order to describe the warping of cross-sections of sandwich and composite beams.

Yu and Hwu (2005) rederived the comprehensive model with finite element method. To show the accuracy and generality of the comprehensive dynamic finite element model for the free vibration analysis of the tapered stiffened composite wing structures, an illustration, for a cantilever NACA 2412 composite wing with uniform chord length along the direction of span is given. Moreover, several numerical results of different tapered ratio wing are introduced to study the influence of tapered effect.

Subramanian (2006) presented dynamic analysis of two different one-dimensional finite element models for laminated composite beams, in which a 5<sup>th</sup> order expansion was

used to expand the axial displacement and a 4<sup>th</sup> order power series was used for the transverse displacement.

Murugan et al (2012) addressed optimal design of laminated composite beams with stiffness and aeroelastic constraints. The design variables were the fiber orientations of the laminate on the walls of the internal blade spar.

Blasques and Stolpe (2012) presented a simultaneous optimization of topology and laminate properties in structural design of laminated composite beam cross sections. The structural response of the beam is evaluated using a beam finite element model. Solutions are presented for a maximum stiffness problem with constraints on the weight, and the shear and mass center positions.

Modal analysis of noncontinuous or stepped beams can be done exactly just for not so complicated systems. If the cross-sections of the beam are very complex, numerical methods are preferred.

In this study, modal analysis of aerofoil cross-sectioned wing made of laminated composite and filled with foam is studied by Finite Element Method with the help of ANSYS which is very powerful and well proven software all around the world. The effects of ratio of overhangs to mid-span and length of the thickened parts on natural frequencies are investigated by finite element models developed in ANSYS and the model is verified by theoretical results available in the literature.

## CHAPTER 2

### THEORETICAL BACKGROUND

#### 2.1. Description of the Problem

The problem is the modal analysis of aerofoil cross-sectioned wing made of laminated composite and filled with foam. The wing has two overhangs as shown in Figure 2.1. In general, wing has two different cross-sections along the longitudinal axis due to the supports and mid part of the beam. It is seen from Figure 2.1 that support regions and mid part are dimensioned as  $L_2$  which are the thickened cross-section parts of the wing.

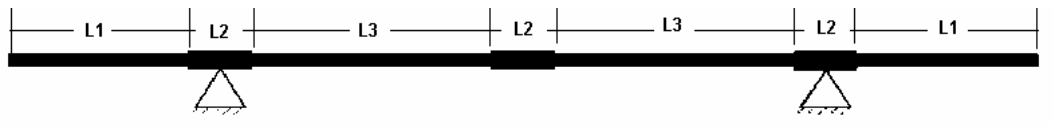


Figure 2.1. A wing with two overhangs

The cross-section of the wing is given in Figure 2.1. Wing surface is based on Laminated Composite 1. All necessary lamina codes and material details are given in the numerical application part of this thesis. Leading edge panel and spar caps have thick pure epoxy. On the other hand, shear web has foam as core material. Moreover, trailing edge reinforcement is made up epoxy.

The difference between the cross-sections of the wing parts having length  $L_1$  &  $L_3$  and  $L_2$  is the lamina code of the Laminated Composite 1 shown in Figure 2.2. Thickened cross-section part of the wing having the length  $L_2$  has more layers than the wing having the length  $L_1$  &  $L_3$ .

In this study, the effects of ratio of overhangs to mid-span  $= (L_1 + L_2/2)/(2L_2 + 2L_3)$  or the ratio of span to length  $= (2L_2 + 2L_3)/(2L_1 + 3L_2 + 2L_3)$  and  $L_2$  on natural frequencies are investigated by finite element models verified by theoretical results available in the literature just for a special case ( $L_2=0$ ).

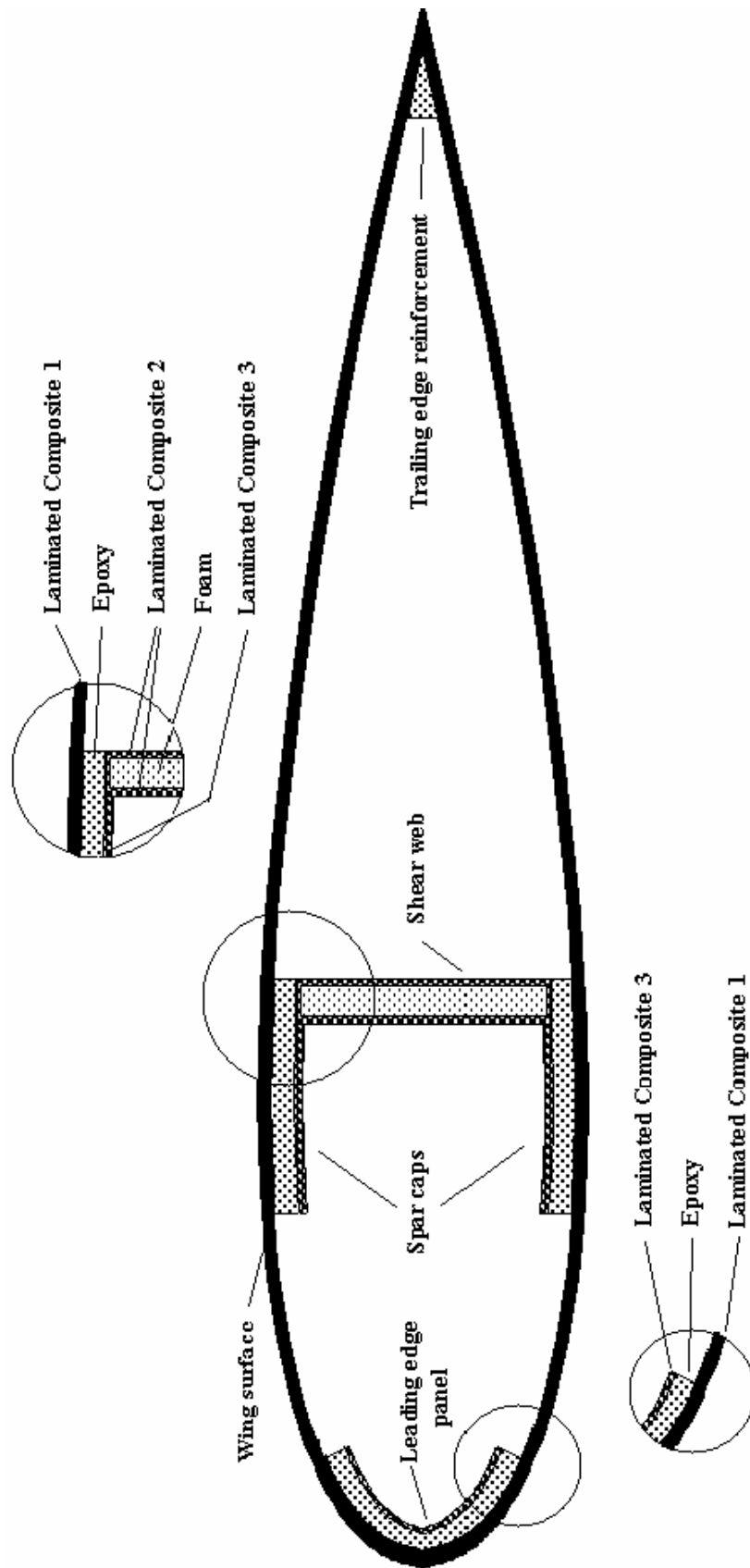


Figure 2.2. Cross-section of the wing

## 2.2. Modal Analysis of Multi-Part Wing

A beam with uniform cross-section having typical boundary conditions is considered. In this case, bending rigidity of the beam  $EI$  along the beam axis is constant. Thus, free bending vibration of a beam is governed by (Inman 2001)

$$EI \frac{\partial^4 v(z,t)}{\partial z^4} + \rho A \frac{\partial^2 v(z,t)}{\partial t^2} = 0 \quad (2.1)$$

where  $E$  is Young's modulus,  $I$  is second moment of area,  $\rho$  is density of the beam and  $A$  is the area of the cross section of the beam. Also,  $v(z,t)$  is the transverse displacement of the beam. Equation (2.1) is reduced to differential eigenvalue problem as

$$\frac{d^4 V(z)}{dz^4} - \beta^4 V(z) = 0 \quad (2.2)$$

$$\beta^4 = \rho A \omega^2 / EI \quad (2.3)$$

where  $\beta$  is non-dimensional natural frequency parameter. The general solution of Equation (2.2) is expressed as

$$V(z) = B_1 \sin \beta z + B_2 \cos \beta z + B_3 \sinh \beta z + B_4 \cosh \beta z \quad (2.4)$$

where  $V(z)$  represents bending mode shapes of the beam. In order to find the non-dimensional natural frequency parameters and the corresponding mode shapes of the beam with typical boundary conditions, boundary conditions are used. For example, if the beam is simply supported at both ends, the following equations are written

$$\text{Deflection} = V(0) = 0 \quad (2.5)$$

$$\text{Bending moment} = EI \left. \frac{d^2 V(z)}{dz^2} \right|_{z=0} = 0$$

Other boundary conditions at  $z = l$  are written similarly.

Four equations from Equation (2.5) provide a system of linear homogeneous equations. In order to find the non-dimensional natural frequency parameters, the determinant of the coefficient matrix of linear homogeneous equations must be zero. Then, frequency equation is determined and solved for  $\beta$ . After finding  $\beta$ , corresponding mode shape function  $V(z)$  is found.

For multi-part wing, Equation (2.4) is written for each part of the beam. Therefore, the number of unknown coefficients is equal to four times number of part. In order to determine the unknown coefficients, boundary conditions of the beam and the continuity conditions between parts are used.

At the junction of two parts; the continuity of deflection, slope, bending moment and shear force must be preserved. Let us consider two parts named as 1 and 2 has a junction at  $z = b$ , aforementioned continuity conditions are written as

$$\text{Deflection} = V_1(b) = V_2(b)$$

$$\text{Slope} = V_1'(b) = V_2'(b)$$

(2.6)

$$\text{Bending moment} = EI_1 \left. \frac{d^2 V_1(z)}{dz^2} \right|_{z=b} = EI_2 \left. \frac{d^2 V_2(z)}{dz^2} \right|_{z=b}$$

$$\text{Shear force} = EI_1 \left. \frac{d^3 V_1(z)}{dz^3} \right|_{z=b} = EI_2 \left. \frac{d^3 V_2(z)}{dz^3} \right|_{z=b}$$

Therefore, for the considered simply supported beam with two parts: there are  $2 \times 4 = 8$  unknown coefficients. Four equations from Equation (2.5) and four equations from Equations (2.6) provide a system of linear homogeneous equations. The solution procedure is the same with the previous one. In order to find the non-dimensional natural frequency parameters, the determinant of the coefficient matrix of linear homogeneous equations must be zero. Then, frequency equation is determined and solved for  $\beta$ . After finding  $\beta$ , corresponding mode shape functions  $V(z)$  for each part are found.

### 2.3. Vibration of Simply Supported Beams with Overhang

The procedure of the transverse vibration analysis of beams with multi-part presented in section 2.2 can be applied to a beam with overhang shown in Figure 2.3.

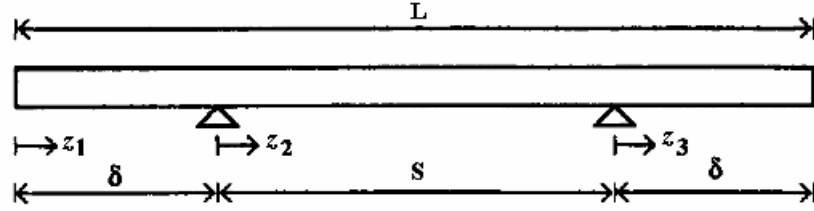


Figure 2.3. Geometry of simply supported beam with symmetric overhang  
(Source: Murphy 1997)

The simply supported continuous beams with symmetric overhang shown in Figure 2.3 can be divided into three parts with three distinct coordinate systems  $z_1$ ,  $z_2$ , and  $z_3$  and origins. Let  $V_1(z)$ ,  $V_2(z)$ , and  $V_3(z)$  be the normal functions of the beam sections (see Equation (2.4) ). The general solution for the normal functions are

$$\begin{aligned} V_1(z_1) &= B_1 \sin \beta z_1 + B_2 \cos \beta z_1 + B_3 \sinh \beta z_1 + B_4 \cosh \beta z_1 \quad 0 \leq z_1 \leq \delta \\ V_2(z_2) &= B_2 \sin \beta z_2 + B_2 \cos \beta z_2 + B_3 \sinh \beta z_2 + B_4 \cosh \beta z_2 \quad 0 \leq z_2 \leq s \\ V_3(z_3) &= B_1 \sin \beta z_3 + B_2 \cos \beta z_3 + B_3 \sinh \beta z_3 + B_4 \cosh \beta z_3 \quad 0 \leq z_3 \leq \delta \end{aligned} \quad (2.7)$$

Along with these three normal functions, boundary and continuity conditions must be satisfied. At the ends of the beam both moment and shear have to be zero. At the supports deflection is zero, slope and moment are continuous. These 12 boundary and continuity conditions are expressed mathematically as follows:

$$\begin{aligned} \left. \frac{d^2 V_1(z_1)}{dz_1^2} \right|_{z_1=0} &= 0 \\ \left. \frac{d^3 V_1(z_1)}{dz_1^3} \right|_{z_1=0} &= 0 \\ V_1(\delta) &= 0 \\ V_2(0) &= 0 \end{aligned}$$

$$\begin{aligned}
\left. \frac{dV_1(z_1)}{dz_1} \right|_{z_1=\delta} - \left. \frac{dV_2(z_2)}{dz_2} \right|_{z_2=0} &= 0 \\
\left. \frac{d^2V_1(z_1)}{dz_1^2} \right|_{z_1=\delta} - \left. \frac{d^2V_2(z_2)}{dz_2^2} \right|_{z_2=0} &= 0 \\
V_2(S) &= 0 \\
V_3(0) &= 0 \\
\left. \frac{dV_2(z_2)}{dz_2} \right|_{z_2=S} - \left. \frac{dV_3(z_3)}{dz_3} \right|_{z_3=0} &= 0 \\
\left. \frac{d^2V_2(z_2)}{dz_2^2} \right|_{z_2=S} - \left. \frac{d^2V_3(z_3)}{dz_3^2} \right|_{z_3=0} &= 0 \\
\left. \frac{d^2V_3(z_3)}{dz_3^2} \right|_{z_3=\delta} &= 0 \\
\left. \frac{d^3V_3(z_3)}{dz_3^3} \right|_{z_3=\delta} &= 0
\end{aligned} \tag{2.8}$$

If  $\alpha = S/L$  is defined as the ratio of span to length, then the overhang can be expressed as  $\delta = L(1 - \alpha)/2$ .

From Equation (2.7), 12 by 12 matrix of the coefficients of the 12 constants can be constructed. The elements of the matrix consist of the trigonometric and hyperbolic terms of the normal functions given in Equation (2.7). This set of homogeneous equations will have nontrivial solutions only if the determinant of the coefficients vanishes. Expansion of the determinant is the frequency equation. Roots of the frequency equation correspond to the natural frequencies. The minimum nonzero  $\beta L$  value that makes the determinant zero is used to calculate the fundamental frequency. From Equation (2.3), natural frequency in Hz is calculated by (Murphy 1997)

$$f = \sqrt{K_1} \sqrt{\frac{EI}{\rho AL^4}} \tag{2.9}$$

where  $K_1$  is transformed fundamental root of the frequency equation and given as



$$K_1 = \left( \frac{(\beta L)^2}{2\pi} \right)^2 \quad (2.10)$$

The variation of transformed fundamental root of the frequency equation  $K_1$  for a simply supported beam with symmetric overhang with the ratio of span to length  $\alpha$  is shown in Figure 2.4.

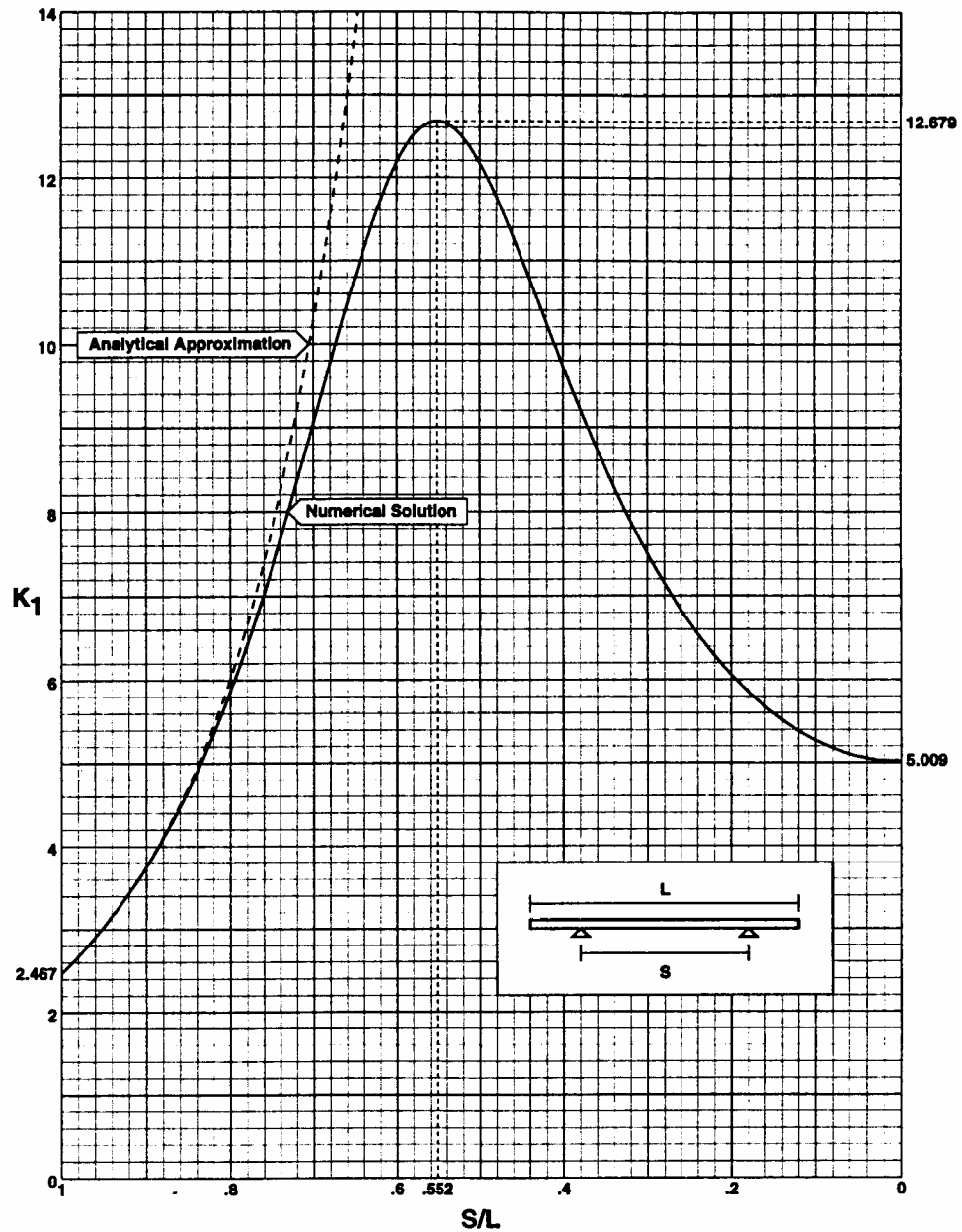


Figure 2.4 Transformed fundamental root of the frequency equation for a simply supported beam with symmetric overhang (Source: Murphy 1997)

## 2.4. Mechanics of Laminated Composites

### 2.4.1. Macromechanical Analysis of a Lamina

In order to understand the stress–strain relationship for an angle lamina in  $x$ - $y$  coordinate system, Figure 2.3 is considered.

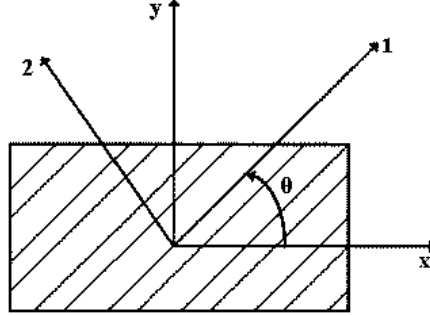


Figure 2.5. Local and global axes of an angle lamina.

The stress–strain relationship in  $x$ - $y$  coordinate system is (Kaw 2006)

$$\begin{Bmatrix} \sigma_x \\ \sigma_y \\ \tau_{xy} \end{Bmatrix} = \begin{bmatrix} \bar{Q}_{11} & \bar{Q}_{12} & \bar{Q}_{16} \\ \bar{Q}_{12} & \bar{Q}_{22} & \bar{Q}_{26} \\ \bar{Q}_{16} & \bar{Q}_{26} & \bar{Q}_{66} \end{bmatrix} \begin{Bmatrix} \varepsilon_x \\ \varepsilon_y \\ \gamma_{xy} \end{Bmatrix} \quad (2.11)$$

where  $\bar{Q}_{ij}$  are given by

$$\bar{Q}_{11} = Q_{11}c^4 + Q_{22}s^4 + 2(Q_{12} + 2Q_{66})s^2c^2 \quad (2.12)$$

$$\bar{Q}_{12} = (Q_{11} + Q_{22} - 4Q_{66})s^2c^2 + Q_{12}(c^4 + s^2) \quad (2.13)$$

$$\bar{Q}_{22} = Q_{11}s^4 + Q_{22}c^4 + 2(Q_{12} + 2Q_{66})s^2c^2 \quad (2.14)$$

$$\bar{Q}_{16} = (Q_{11} - Q_{12} - 2Q_{66})c^3s - (Q_{22} - Q_{12} - 2Q_{66})s^3c \quad (2.15)$$

$$\bar{Q}_{26} = (Q_{11} - Q_{12} - 2Q_{66})cs^3 - (Q_{22} - Q_{12} - 2Q_{66})sc^3 \quad (2.16)$$

$$\bar{Q}_{66} = (Q_{11} + Q_{22} - 2Q_{12} - 2Q_{66})c^2s^2 + Q_{66}(s^4 + c^4) \quad (2.17)$$

in which  $c=\text{Cos}(\theta)$  and  $s=\text{Sin}(\theta)$  The stiffness coefficients  $Q_{ij}$  are related to the engineering constants and given as:

$$Q_{11} = \frac{E_1}{1 - \nu_{21}\nu_{12}} \quad (2.18)$$

$$Q_{12} = \frac{\nu_{12}E_2}{1 - \nu_{21}\nu_{12}} \quad (2.19)$$

$$Q_{22} = \frac{E_2}{1 - \nu_{21}\nu_{12}} \quad (2.20)$$

$$Q_{66} = G_{12} \quad (2.21)$$

Since the  $\bar{Q}_{ij}$  presented above do not allow a direct study of the effect of the angle of the lamina on the  $\bar{Q}_{ij}$ , they can be written in invariant form as

$$\bar{Q}_{11} = U_1 + U_2 \text{Cos}2\theta + U_3 \text{Cos}4\theta \quad (2.22)$$

$$\bar{Q}_{12} = U_4 - U_3 \text{Cos}4\theta \quad (2.23)$$

$$\bar{Q}_{22} = U_1 - U_2 \text{Cos}2\theta + U_3 \text{Cos}4\theta \quad (2.24)$$

$$Q_{16} = \frac{U_2}{2} \text{Sin}2\theta + U_3 \text{Sin}4\theta \quad (2.25)$$

$$Q_{26} = \frac{U_2}{2} \text{Sin}2\theta - U_3 \text{Sin}4\theta \quad (2.26)$$

$$\bar{Q}_{66} = \frac{1}{2}(U_1 - U_4) - U_3 \cos 4\theta \quad (2.27)$$

where

$$U_1 = \frac{1}{8}(3Q_{11} + 3Q_{22} + 2Q_{12} + 4Q_{66}) \quad (2.28)$$

$$U_2 = \frac{1}{2}(Q_{11} - Q_{22}) \quad (2.29)$$

$$U_3 = \frac{1}{8}(3Q_{11} + Q_{22} - 2Q_{12} - 4Q_{66}) \quad (2.30)$$

$$U_4 = \frac{1}{8}(Q_{11} + Q_{22} + 6Q_{12} - 4Q_{66}) \quad (2.31)$$

## 2.4.2 Macromechanical Analysis of Laminates

A laminate is made of a group of single layers bonded to each other as shown in Figure 2.6. Special notations are used for the laminate code. For example:  $[0/-45/60]_s$

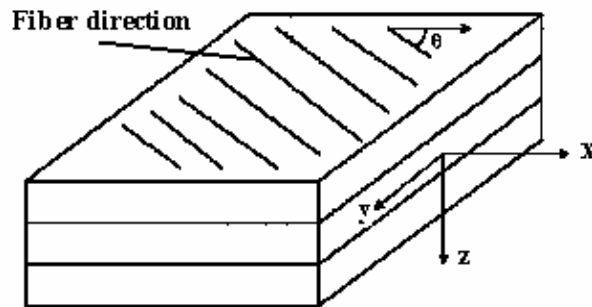
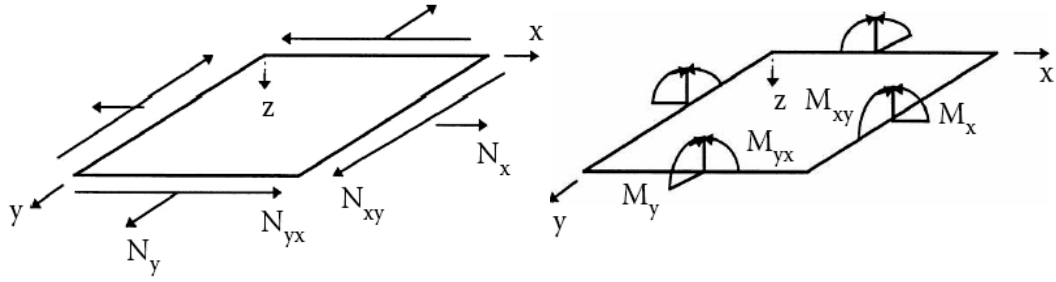


Figure 2.6. Schematic of a laminate.

In this section, the classical lamination theory for a plate under the in-plane loads shown in Figure 2.7 is presented.



$N_x, N_y$  = normal force per unit length,  $N_{xy}$  = shear force per unit length  
 $M_x, M_y$  = bending moments per unit length,  $M_{xy}$  = twisting moments per unit length

Figure 2.7. Resultant forces and moments on a laminate.

The strain-displacement equations can be written in matrix form as:

$$\begin{Bmatrix} \varepsilon_x \\ \varepsilon_y \\ \gamma_{xy} \end{Bmatrix} = \begin{Bmatrix} \varepsilon_x^0 \\ \varepsilon_y^0 \\ \gamma_{xy}^0 \end{Bmatrix} + z \begin{Bmatrix} \kappa_x \\ \kappa_y \\ \kappa_{xy} \end{Bmatrix} \quad (2.32)$$

where the midplane strains and curvatures are given as

$$\begin{Bmatrix} \varepsilon_x^0 \\ \varepsilon_y^0 \\ \gamma_{xy}^0 \end{Bmatrix} = \begin{Bmatrix} \frac{\partial u_0}{\partial x} \\ \frac{\partial v_0}{\partial y} \\ \frac{\partial u_0}{\partial y} + \frac{\partial v_0}{\partial x} \end{Bmatrix} \quad (2.33)$$

$$\begin{Bmatrix} \kappa_x \\ \kappa_y \\ \kappa_{xy} \end{Bmatrix} = \begin{Bmatrix} \frac{\partial^2 w_0}{\partial x^2} \\ \frac{\partial^2 w_0}{\partial y^2} \\ -2 \frac{\partial^2 w_0}{\partial x \partial y} \end{Bmatrix} \quad (2.34)$$

Let us consider a laminate made of  $n$  plies shown in Figure 2.8. Each ply has a thickness of  $t_k$ . Then the thickness of the laminate  $h$  is

$$h = \sum_{k=1}^n t_k \quad (2.35)$$

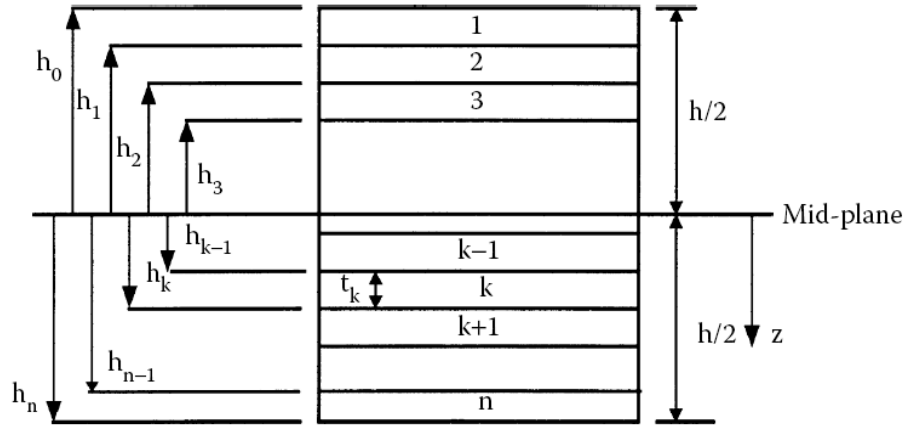


Figure 2.8. Coordinate locations of plies in a laminate.

The forces and moments in the plate having thickness  $h$  are written as

$$\begin{bmatrix} N_x \\ N_y \\ N_{xy} \end{bmatrix} = \int_{-h/2}^{h/2} \begin{bmatrix} \sigma_x \\ \sigma_y \\ \tau_{xy} \end{bmatrix} dz \quad (2.36)$$

$$\begin{bmatrix} M_x \\ M_y \\ M_{xy} \end{bmatrix} = \int_{-h/2}^{h/2} \begin{bmatrix} \sigma_x \\ \sigma_y \\ \tau_{xy} \end{bmatrix} z dz \quad (2.37)$$

Since the laminate made of  $n$  plies, forces and moments in each lamina are summed after integrating the stresses for each lamina to give the resultant forces and moments in the laminate as

$$\begin{bmatrix} N_x \\ N_y \\ N_{xy} \end{bmatrix} = \sum_{k=1}^n \int_{h_{k-1}}^{h_k} \begin{bmatrix} \sigma_x \\ \sigma_y \\ \tau_{xy} \end{bmatrix}_k dz \quad (2.38)$$

$$\begin{bmatrix} M_x \\ M_y \\ M_{xy} \end{bmatrix} = \sum_{k=1}^n \int_{h_{k-1}}^{h_k} \begin{bmatrix} \sigma_x \\ \sigma_y \\ \tau_{xy} \end{bmatrix}_k z dz \quad (2.39)$$

Now, the resultant forces and moments are written in terms of the midplane strains and curvatures by using the stress–strain relationship as

$$\begin{bmatrix} N_x \\ N_y \\ N_{xy} \end{bmatrix} = \begin{bmatrix} A_{11} & A_{12} & A_{16} \\ A_{12} & A_{22} & A_{26} \\ A_{16} & A_{26} & A_{66} \end{bmatrix} \begin{bmatrix} \varepsilon_x^0 \\ \varepsilon_y^0 \\ \gamma_{xy}^0 \end{bmatrix} + \begin{bmatrix} B_{11} & B_{12} & B_{16} \\ B_{12} & B_{22} & B_{26} \\ B_{16} & B_{26} & B_{66} \end{bmatrix} \begin{bmatrix} \kappa_x \\ \kappa_y \\ \kappa_{xy} \end{bmatrix} \quad (2.40)$$

$$\begin{bmatrix} M_x \\ M_y \\ M_{xy} \end{bmatrix} = \begin{bmatrix} B_{11} & B_{12} & B_{16} \\ B_{12} & B_{22} & B_{26} \\ B_{16} & B_{26} & B_{66} \end{bmatrix} \begin{bmatrix} \varepsilon_x^0 \\ \varepsilon_y^0 \\ \gamma_{xy}^0 \end{bmatrix} + \begin{bmatrix} D_{11} & D_{12} & D_{16} \\ D_{12} & D_{22} & D_{26} \\ D_{16} & D_{26} & D_{66} \end{bmatrix} \begin{bmatrix} \kappa_x \\ \kappa_y \\ \kappa_{xy} \end{bmatrix} \quad (2.41)$$

where the  $[A]$ ,  $[B]$ , and  $[D]$  matrices are called the extensional, coupling, and bending stiffness matrices, respectively. The matrix  $[A]$  relates the resultant in-plane forces to the in-plane strains, and the matrix  $[D]$  relates the resultant bending moments to the plate curvatures. The matrix  $[B]$  couples the force and moment terms to the midplane strains and midplane curvatures. Elements of the  $[A]$ ,  $[B]$ , and  $[D]$  are given as

$$A_{ij} = \sum_{k=1}^n [(\bar{Q}_{ij})]_k (h_k - h_{k-1}), \quad i = 1,2,6; \quad j = 1,2,6 \quad (2.42)$$

$$B_{ij} = \frac{1}{2} \sum_{k=1}^n [(\bar{Q}_{ij})]_k (h_k^2 - h_{k-1}^2), \quad i = 1,2,6; \quad j = 1,2,6 \quad (2.43)$$

$$D_{ij} = \frac{1}{3} \sum_{k=1}^n [(\bar{Q}_{ij})]_k (h_k^3 - h_{k-1}^3), \quad i = 1,2,6; \quad j = 1,2,6 \quad (2.44)$$

### 2.4.3. Material Properties of Cross-Section of the Wing

Detailed cross-section of the wing is given in Figure 2.2. In order to model the wing as beam, mass and stiffness properties of the wing can be obtained by using the equivalent system approach. To do this, Figure 2.2 is modified by numbering the each part of the cross-section and this is shown in Figure 2.9.

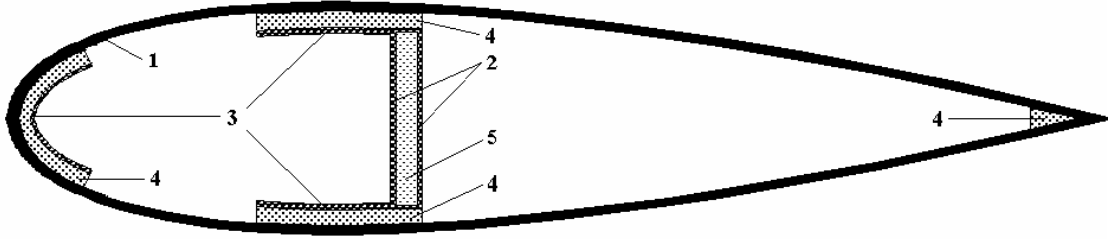


Figure 2.9 Parts of the cross-section of the wing in  $x$ - $y$  plane

Equivalent mass density of the wing can be obtained by using the following equation:

$$\rho_e = \frac{\rho_1 A_1 + \rho_2 A_2 + \rho_3 A_3 + \rho_4 A_4 + \rho_5 A_5}{A_1 + A_2 + A_3 + A_4 + A_5} \quad (2.45)$$

where  $\rho_i$  and  $A_i$  are density and cross-sectional area of the  $i^{\text{th}}$  part ( $i=1, 2, 3, 4, 5$ ).

Similarly, equivalent modulus of elasticity in the direction of longitudinal axis of the wing can be obtained as follows:

$$E_{ea} = \frac{E_{z1} A_1 + E_{z2} A_2 + E_{z3} A_3 + E_{z4} A_4 + E_{z5} A_5}{A_1 + A_2 + A_3 + A_4 + A_5} \quad (2.46)$$

where  $E_i$  is the modulus of elasticity of the  $i^{\text{th}}$  part ( $i=1, 2, 3, 4, 5$ ) of the wing in the longitudinal axis of the wing.

Also, equivalent modulus of elasticity in the direction of longitudinal axis of the wing due to bending about  $x$  axis can be obtained as follows:



$$E_{ebx} = \frac{E_{1z}I_{1xx} + E_{2z}I_{2xx} + E_{3z}I_{3xx} + E_{4z}I_{4xx} + E_{5z}I_{5xx}}{I_{1xx} + I_{2xx} + I_{3xx} + I_{4xx} + I_{5xx}} \quad (2.47)$$

where  $E_i$  is the modulus of elasticity of the  $i^{\text{th}}$  part ( $i=1, 2, 3, 4, 5$ ) of the wing in the longitudinal axis of the wing.

Moreover, equivalent modulus of elasticity in the direction of longitudinal axis of the wing due to bending about  $y$  axis can be obtained as follows:

$$E_{eby} = \frac{E_{1z}I_{1yy} + E_{2z}I_{2yy} + E_{3z}I_{3yy} + E_{4z}I_{4yy} + E_{5z}I_{5yy}}{I_{1yy} + I_{2yy} + I_{3yy} + I_{4yy} + I_{5yy}} \quad (2.48)$$

where  $E_i$  is the modulus of elasticity of the  $i^{\text{th}}$  part ( $i=1, 2, 3, 4, 5$ ) of the wing in the longitudinal axis of the wing.

## 2.5. Modal Analysis by Finite Element Method

The equation of motion of discrete system is given by

$$[M]\{\ddot{x}(t)\} + [D]\{\dot{x}(t)\} + ([K] + [G])\{x(t)\} = \{f(t)\} \quad (2.49)$$

where  $[M]$ ,  $[D]$ ,  $[K]$  and  $[G]$  are mass, damping, elastic stiffness and geometric matrices, respectively. It is known that,  $\{x(t)\}$  is displacement vector and  $\{f(t)\}$  is force vector. The equation (2.49) is reduced to generalized eigenvalue equation:

$$([K] + [G] - \omega_i^2[M])\{u_i\} = \{0\} \quad (2.50)$$

where  $\omega_i$  is  $i^{\text{th}}$  natural frequency and  $\{u_i\}$  is the  $i^{\text{th}}$  vibration mode shape vector.

Possible motions related to the mode shape can be seen from Figure 2.10. The motions are named as flapping, lead-lag and torsional motions. Flapping and lead-lag motions are also called as flapwise and chordwise bending, respectively.

It is possible to model the wing by finite element method in several ways based on element type and solution approach. For example, linear layered structural shell element SHELL99 can be used. This element is defined by 8 nodes, average or corner layer

thicknesses, layer material direction angles, orthotropic material properties. Another approach is the usage of beam element BEAM44 based on the equivalent isotropic material for the combination of laminated composite, foam and epoxy used in the wing cross-section.

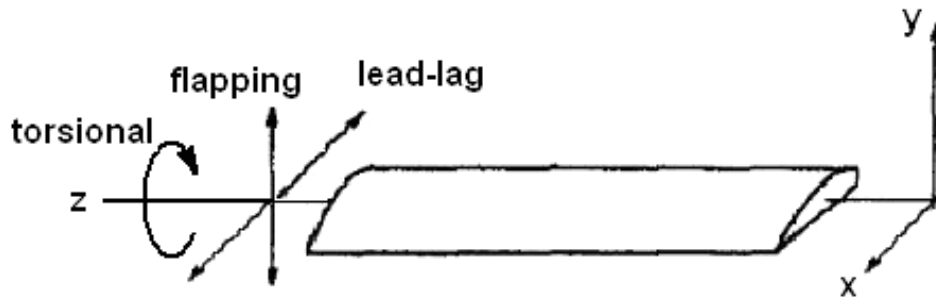


Figure 2.10: Flapping lead-lag and torsional motions of a beam  
(Source: Stafford and Giurgiutiu 1975)

The best modelling can be done in ANSYS by using parametric design language shortened as APDL.

## CHAPTER 3

### NUMERICAL RESULTS AND DISCUSSIONS

#### 3.1. Geometrical Model of the Wing

Wing with two equal overhangs shown in Figure 3.1 has two different aerofoil cross-sections as mentioned earlier. The lengths of the parts of beam are shown in Figure 3.1.

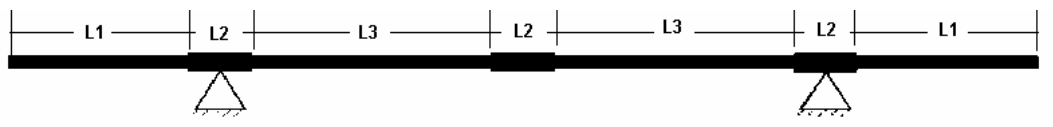
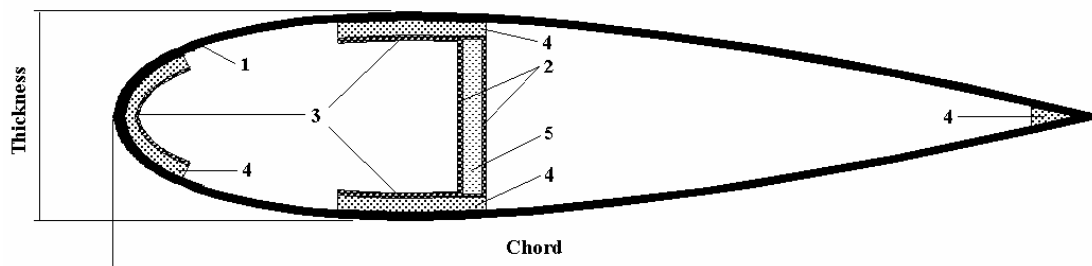


Figure 3.1. Dimensions of the wing with two equal overhangs

Left and right supports of the wing are located at the mid points of the parts having length  $L2$ . Chord and thickness of the aerofoil cross-sectioned wing are shown in Figure 3.2 and given as Chord = 400 mm and Thickness = 82 mm.



Part 1: Laminated composite 1 (LC1)

Part 2: Laminated composite 2 (LC2)

Part 3: Laminated composite 3 (LC3)

Part 4: Epoxy

Part 5: Foam

Figure 3.2. Cross-section of the wing with part numbers

Geometrical properties of each part are given in Table 3.1 and Table 3.2.

Table 3.1 Geometrical properties of each part for *thickness of Part 1a = 3.2 mm*

	$A$ (mm <sup>2</sup> )	$I_{xx}$ (mm <sup>4</sup> )	$I_{yy}$ (mm <sup>4</sup> )
Part 1a: Gelcoat of LC* 1	341.24	3.1368e5	5.3009e6
Part 1b: Layers of LC 1	2347.96	1.94432e6	3.67731e7
Part 2: LC 2	97.939	30593	18011
Part 3: LC 3	287.85	2.0550e5	2.1880e6
Part 4: Epoxy	1092.2	1.0036e6	8.3138e6
Part 5: Foam	636.73	1.9889e5	1.0285e5
All parts	4804.6	3.6973e6	5.2675e7

\* LC means Laminated Composite

Table 3.2 Geometrical properties of each part for *thickness of Part 1b = 5 mm*

	$A$ (mm <sup>2</sup> )	$I_{xx}$ (mm <sup>4</sup> )	$I_{yy}$ (mm <sup>4</sup> )
Part 1a: Gelcoat of LC 1	341.24	3.1368e5	5.3009e6
Part 1b: Layers of LC 1	3733.46	3.02262e6	5.17311e7
Part 2: LC 2	97.939	30593	55429
Part 3: LC 3	287.85	2.0550e5	2.6395e6
Part 4: Epoxy	746.48	6.6671e5	6.4906e6
Part 5: Foam	636.73	1.9889e5	3.4614e5
All parts	5844.3	4.4386e6	6.6564e7

Two types of aerofoil cross-sections of the wing of which data provided above are formed in CAD program and igs files are obtained. Then, importing igs files to ANSYS, the Real Constants used by BEAM44 are obtained. The details of the real constants and the corresponding numerical values of the present two models are given below:

Real Constants used by BEAM44

AREA1, IZ1, IY1, TKZB1, TKYB1, IX1,  
 AREA2, IZ2, IY2, TKZB2, TKYB2, IX2,  
 DX1, DY1, DZ1, DX2, DY2, DZ2,  
 SHEARZ, SHEARY, TKZT1, TKYT1, TKZT2, TKYT2,  
 ARESZ1, ARESY1, ARESZ2, ARESY2, TSF1, TSF2,  
 DSCZ1, DSCY1, DSCZ2, DSCY2, EFSZ, EFSY,  
 Y1, Z1, Y2, Z2, Y3, Z3,  
 Y4, Z4, Y1, Z1, Y2, Z2,  
 Y3, Z3, Y4, Z4, THETA, ISTRN,  
 ADDMAS

Real Constants for *thickness of Part 1a = 3.2 mm*:

R,1,4805.1,0.52679E+08,0.36976E+07,41.968,156.45,0.93070E+07  
 RMORE,4805.1,0.52679E+08,0.36976E+07,41.968,156.45,0.93070E+07  
 RMORE,0.0000,0.0000,0.0000,0.0000,0.0000,0.0000  
 RMORE,1.9010,5.3291,41.968,243.80,41.968,243.80  
 RMORE,0.0000,0.0000,0.0000,0.0000,0.0000,0.0000  
 RMORE,0.35880E-03,-19.795,0.35880E-03,-19.795,0.0000,0.0000

Real Constants for *thickness of Part 1b = 5 mm*:

R,2,5836.5,0.66241E+08,0.44381E+07,41.968,166.95,0.12765E+08  
 RMORE,5836.5,0.66241E+08,0.44381E+07,41.968,166.95,0.12765E+08  
 RMORE,0.0000,0.0000,0.0000,0.0000,0.0000,0.0000  
 RMORE,1.5858,6.0767,41.968,233.30,41.968,233.30  
 RMORE,0.0000,0.0000,0.0000,0.0000,0.0000,0.0000  
 RMORE,0.46510E-03,-32.912,0.46510E-03,-32.912,0.0000,0.0000

### 3.2. Material Models of the Wing

The parts listed in Figure 3.2 are detailed in this section. The cross-section of the wing with 3.2 mm for thickness of Part 1a is named as C-S1 (Cross-Section1). Another one, Part 1b, is named C-S2. Laminate codes and layer thicknesses for C-S1 and C-S2 are given in Tables 3.3 and Table 3.4, respectively.

Table 3.3 Laminate codes and layer thicknesses for C-S1

	Laminate code	Layer thicknesses (mm)
Layers of LC 1	[45/-45/45/0/-45/45/90/-45] <sub>T</sub>	0.4, 0.4, 0.4, 0.2, 0.4, 0.4, 0.2, 0.4
LC 2	[45/-45] <sub>T</sub>	0.4, 0.4
LC 3	[45/-45/45/-45] <sub>T</sub>	0.4, 0.4, 0.4, 0.4

Table 3.4 Laminate codes and layer thicknesses for C-S2

	Laminate code	Layer thicknesses (mm)
Layers of LC 1	[45/-45/45/0/-45/45/90/-45/ 45/0/-45/45/-45] <sub>T</sub>	0.4, 0.4, 0.4, 0.2, 0.4, 0.4, 0.2, 0.4, 0.4, 0.2, 0.4, 0.4, 0.4
LC 2	[45/-45] <sub>T</sub>	0.4, 0.4
LC 3	[45/-45/45/-45] <sub>T</sub>	0.4, 0.4, 0.4, 0.4

Scotchply type 1002 glass/epoxy material is used for all laminated composite parts of the C-S1 and C-S2. Its engineering constants are given by Tsai (1980)

Longitudinal Young's modulus  $E_x = 38.6$  GPa

Transverse Young's modulus  $E_y = 8.27$  GPa

Longitudinal Poisson's ratio  $\nu_x = 0.26$

Longitudinal-transverse shear modulus  $E_s = 4.14$  GPa

Fiber volume fraction  $\nu_f = 0.45$

Specific gravity = 1.8

Also, the typical properties of epoxy which is used as the matrix material and filling are given by Kaw (2006) as follows:

Axial modulus  $E_x = 3.4$  GPa

Transverse modulus  $E_y = 3.4$  GPa

Axial Poisson's ratio  $\nu_x = 0.3$

Axial shear modulus  $E_s = 1.308$  GPa

Specific gravity = 1.2

Airex C70.55 made by Airex is selected as foam material. Its properties are listed below:

Density  $\rho = 60$  kg/m<sup>3</sup>

Tensile modulus in the plane  $E_x = 45$  MPa

Shear modulus  $E_s = 22$  MPa

Poisson's ratio  $\nu_x = 0.32$

Using the equations given in Section 2.2.1 and 2.2.2, axial Young's modulus and shear modulus of each part having laminations which are based on  $A_{11}$  and  $A_{66}$  can be calculated. For this purpose, a computing code is developed by Matlab<sup>®</sup>. The results are given in Table 3.5.

Table 3.5 Axial and shear modulus

	$E_x$ (MPa)	$G_{xy}$ (MPa)
LC 1-CS1	19.758	10.922
LC 1-CS2	20.406	11.02
LC 2	18.628	12.053
LC 3	18.628	12.053

By using the Equations (2.35)-(2.38) along with the data provided in this Chapter, equivalent densities and longitudinal Young's modulus of the C-S1 and C-S12 are found. The results are given in Table 3.6.

Table 3.6 Eqv (equivalent) densities and axial Young's modulus

	C-S1	C-S2
Eqv density $\rho$ (kg/m <sup>3</sup> )	1390	1499
Eqv axial Young's modulus by using $A_i^* E_{ea}$ (GPa)	12.173	14.491
Eqv lateral Young's modulus by using $I_{xxi}^* E_{bx}$ (GPa)	12.796	15.201
Eqv lateral Young's modulus by using $I_{yyi}^* E_{by}$ (GPa)	15.445	16.712

\* related with  $i$ -th part

### 3.3. Verification of the Present Model

To verify the used approach and the finite element model based on beam element BEAM44, due to the lack of information in the existing literature, transverse vibration of the uniform cross-sectioned wing with equal overhangs which is the fundamental part of the study is considered and examined.

The lengths of the wing shown in Figure 3.1 are given again in Figure 3.3 in the modified form and their details are  $L1 = 1650$  mm,  $L3 = 2350$  mm. C-S1 is selected for the cross-section of the wing. After several convergence test, total  $N=20$  beam elements BEAM44 are used for finite element model. The overhangs and span parts of the beam are divided into 4 and 12 elements, respectively. The results of the covergency tests done for finding the proper number of elements necessary to model the beam with two equal overhangs correctly are shown in graphical form in Figure 3.4.

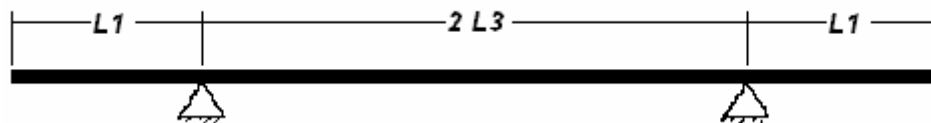


Figure 3.3. Dimensions of the uniform wing with two equal overhangs



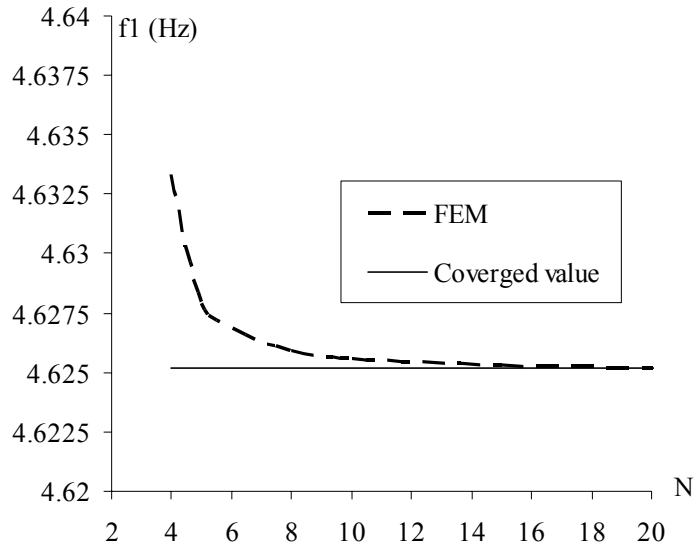


Figure 3.4. Convergence curve

By using the ratio of span to length  $\alpha = S/L$  defined by Murphy (1997) (see Section 2.3 of this thesis) as  $\alpha = 2L3/(2L1+2L3)=4700/8000=0.5875$  is found for the beam shown in Figure 3.3. The transformed fundamental root of the frequency equation  $K_1$  is read from Figure 2.4 approximately 12.3 for  $\alpha = 0.5875$ . Thus, natural frequency  $f$  in Hz is calculated by using Equations (2.9) as  $f=4.76926$  Hz.

The present finite element results and the results available in the literature are given in Table 3.7.

Table 3.7 Comparisons of natural frequencies (Hz)

	Present, N=20	Rao and Rao (1973)	Murphy (1997)
First natural frequency $f_1$	4.6252	4.639	4.76926
Second natural frequency $f_2$	9.6614	10.1063	-
Third natural frequency $f_3$	15.078	16.2629	-

It can be seen from Table 3.7 that present results are in good agreement with the results obtained from the available in the literature.

The natural mode shapes of the natural frequencies presented in Table 3.7 are plotted in the Figure 3.5 to Figure 3.7.

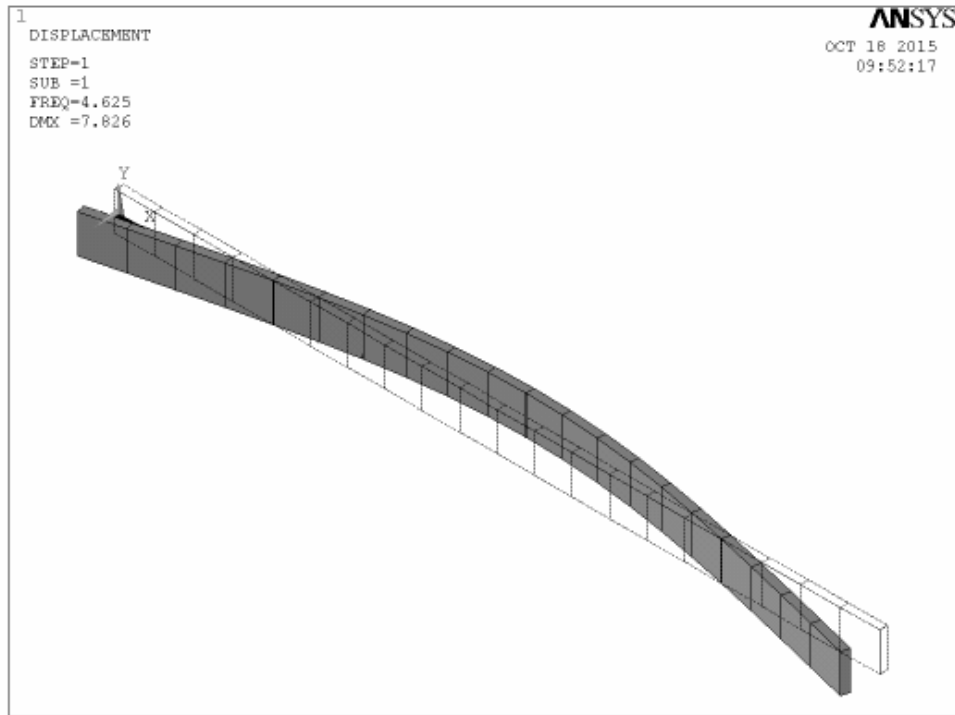


Figure 3.5. First natural mode shape: Flapping 1

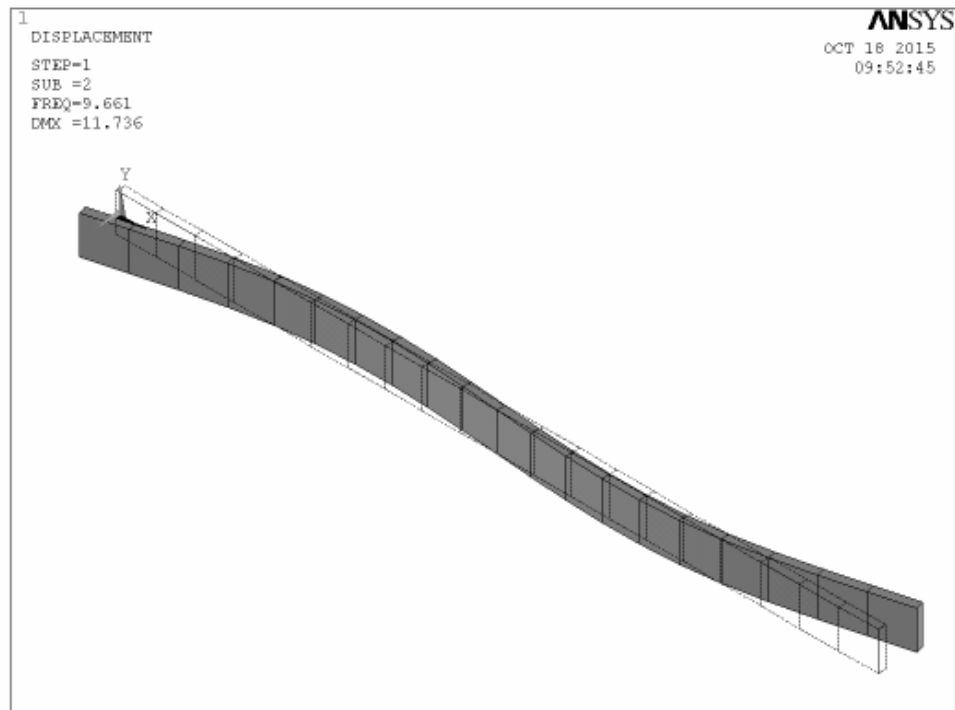


Figure 3.6. Second natural mode shape: Flapping 2

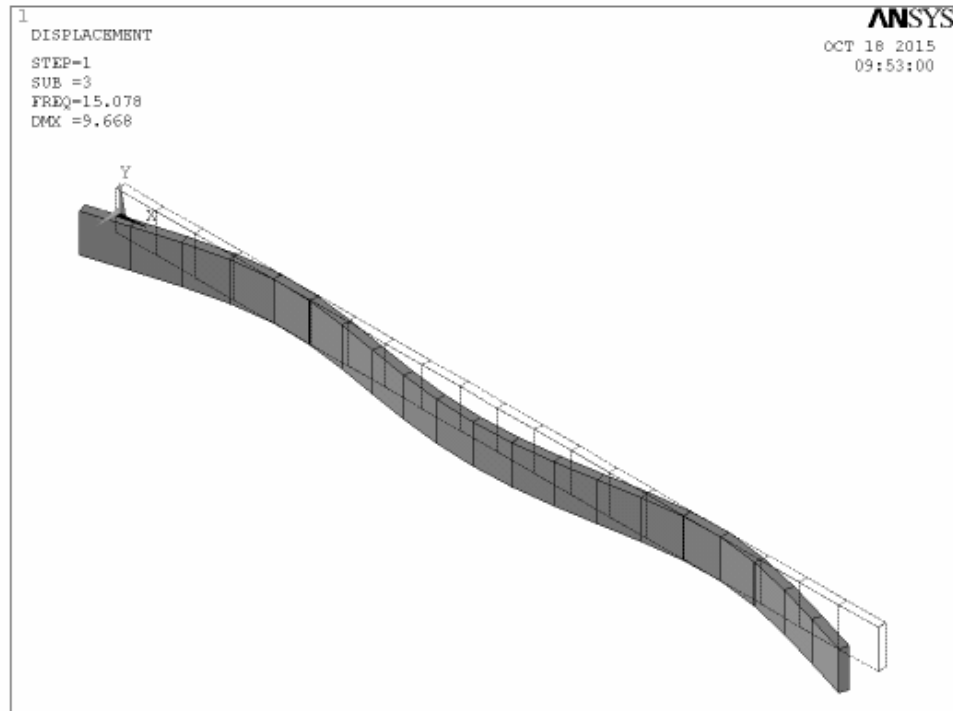


Figure 3.7. Third natural mode shape: Flapping 3

### 3.4. Natural Frequencies and Mode Shapes of Main Model

The main model, shown in Figure 3.8, with lengths  $L1 = 1400$  mm,  $L2 = 500$  mm and  $L3 = 1850$  mm are considered in this section. In this model, the effects of the thickened parts on natural frequencies are studied. In order to get accurate results for higher order natural frequencies,  $N=40$  elements are used to model the beam after checking the convergency for higher order natural frequencies. The natural frequencies of uniform wing and multi-section wing are given in Table 3.8. Only the mode shapes of multi-section wing are given in Figures 3.9-3.20.

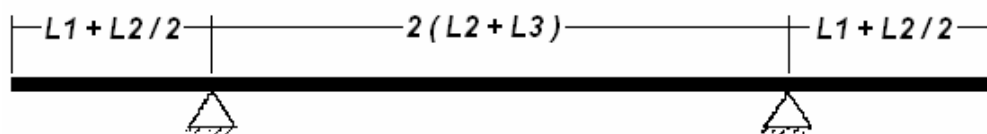


Figure 3.8. Dimensions of the wing with two equal overhangs

Table 3.8. Natural frequencies $f_i$ (Hz) with N=40 elements		
Mode shapes	Uniform Wing	Multi-Section Wing
Flapping 1	4.6252	4.6906
Flapping 2	9.6611	10.136
Flapping 3	15.077	15.996
Lead-Lag 1	17.316	17.624
Flapping 4	31.050	32.126
Lead-Lag 2	35.601	37.563
Flapping 5	54.397	58.107
Lead-Lag 3	58.156	58.918
Flapping 6	81.385	81.759
Flapping 7	81.423	82.040

As expected, it is seen from Table 3.8 that multi-section wing with the strengthened cross sections have higher natural frequencies than the wing with uniform cross-section.

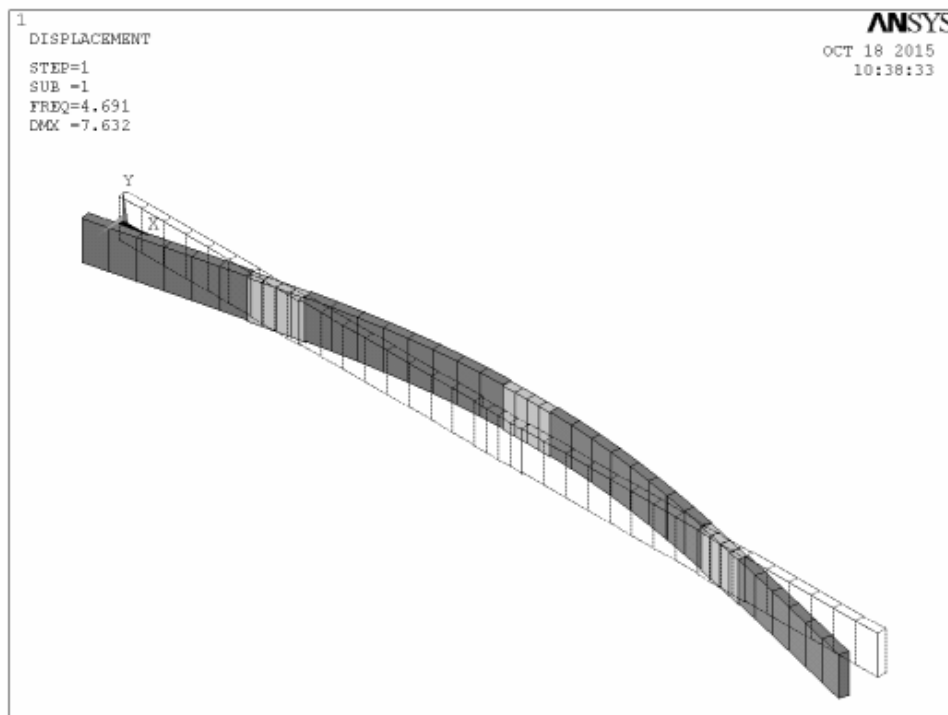


Figure 3.9. Flapping 1

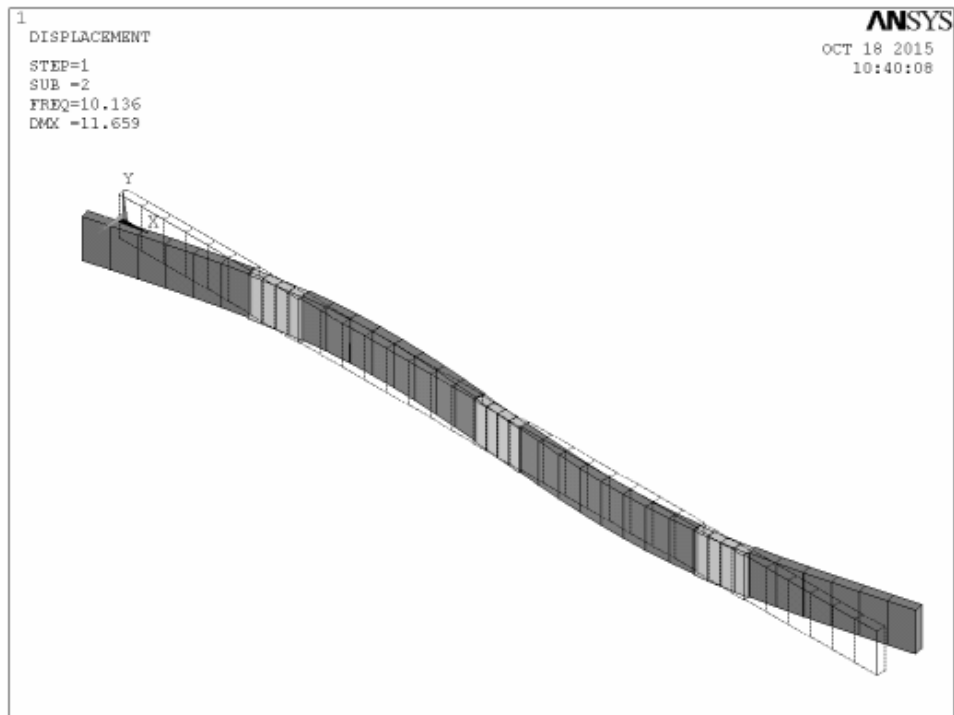


Figure 3.10. Flapping 2

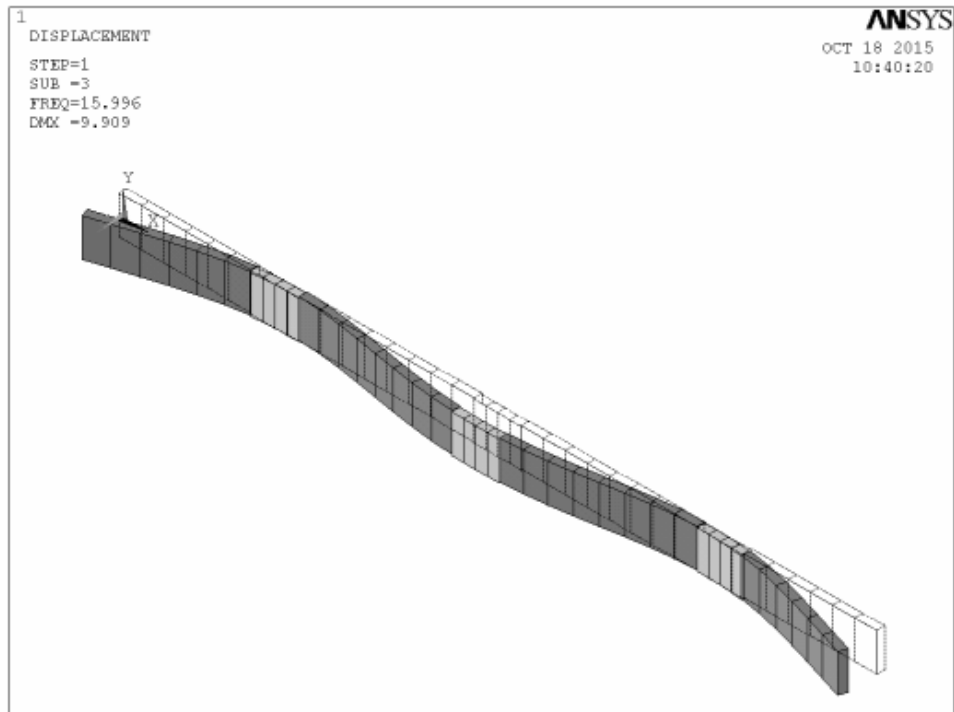


Figure 3.11. Flapping 3

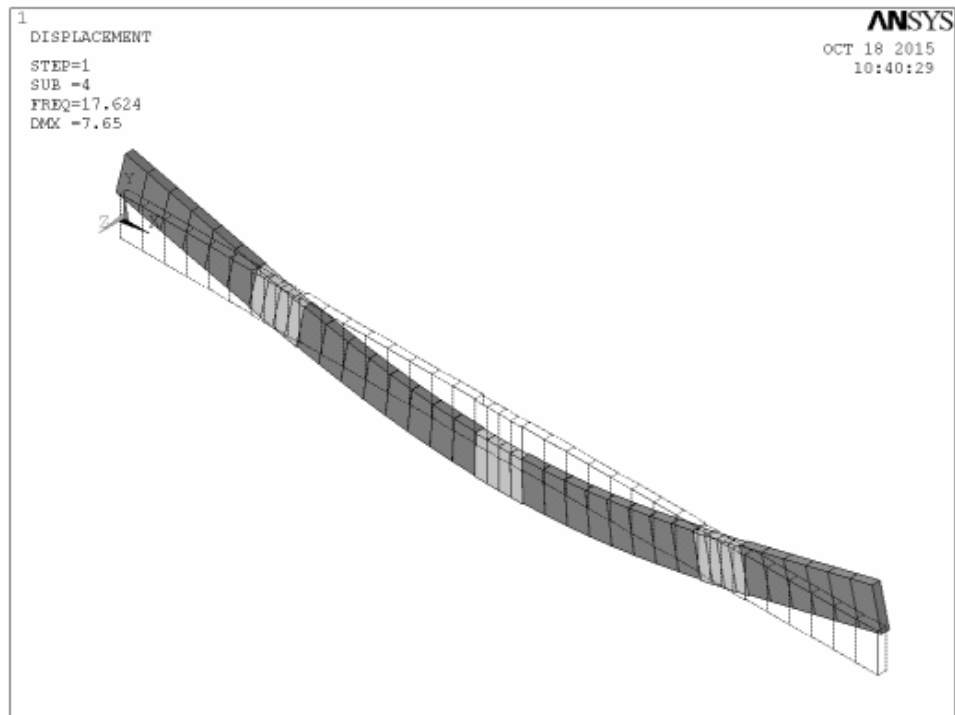


Figure 3.12. Lead-Lag 1

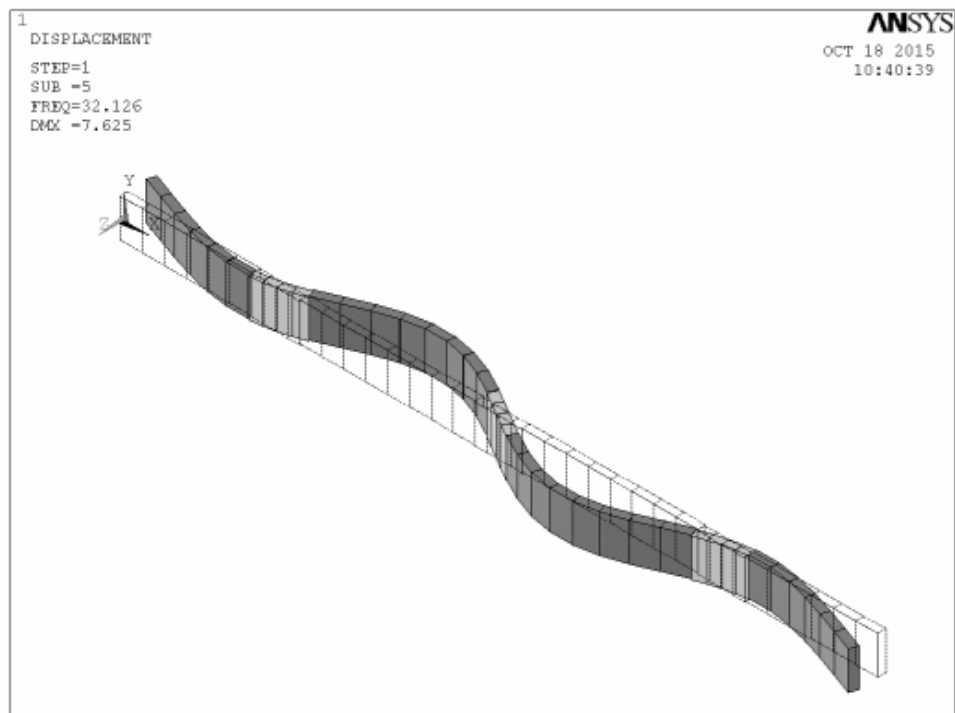


Figure 3.13. Flapping 4

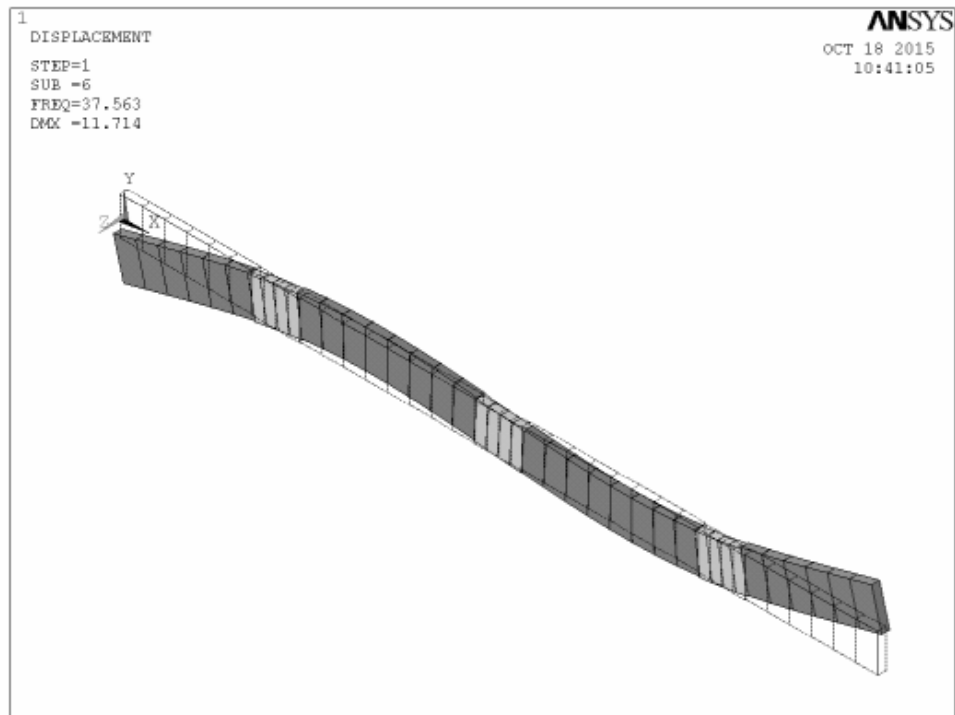


Figure 3.14. Lead-Lag 2

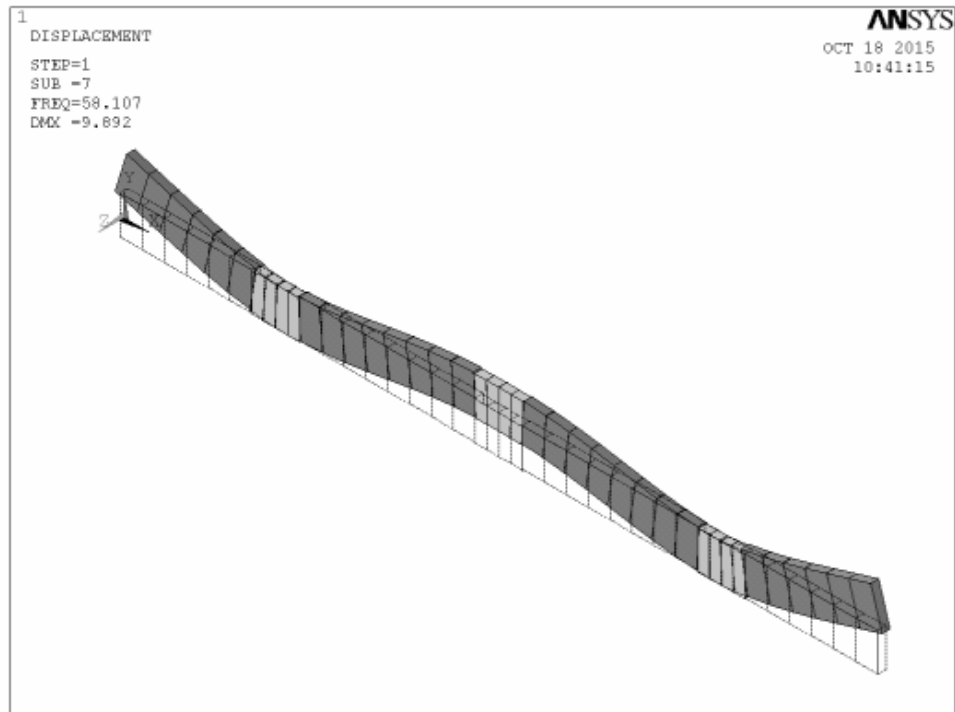


Figure 3.15. Lead-Lag 3

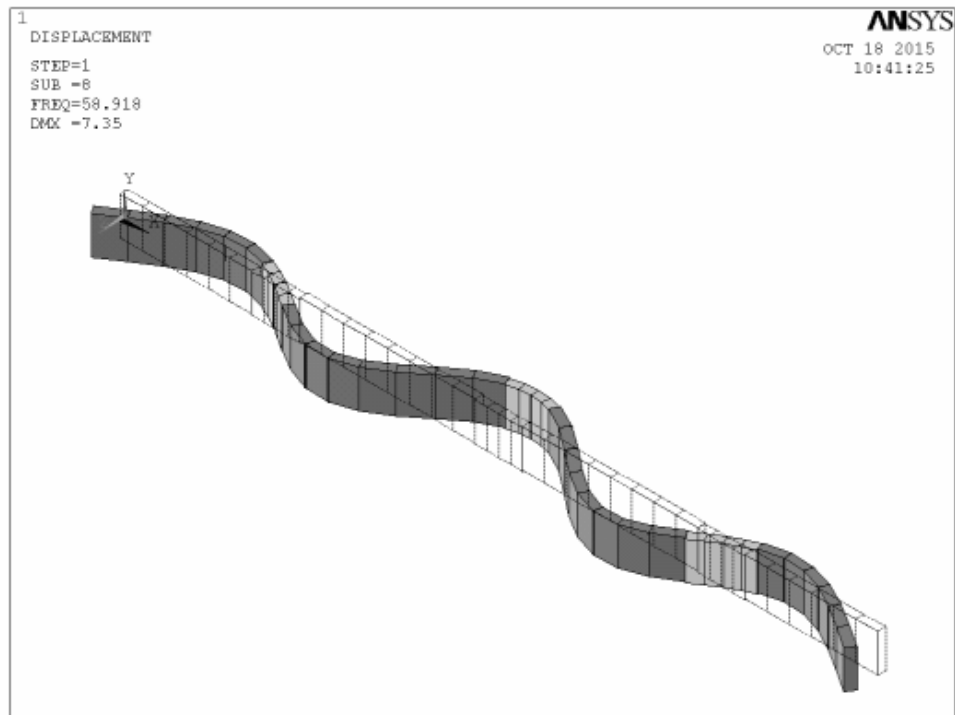


Figure 3.16. Flapping 5

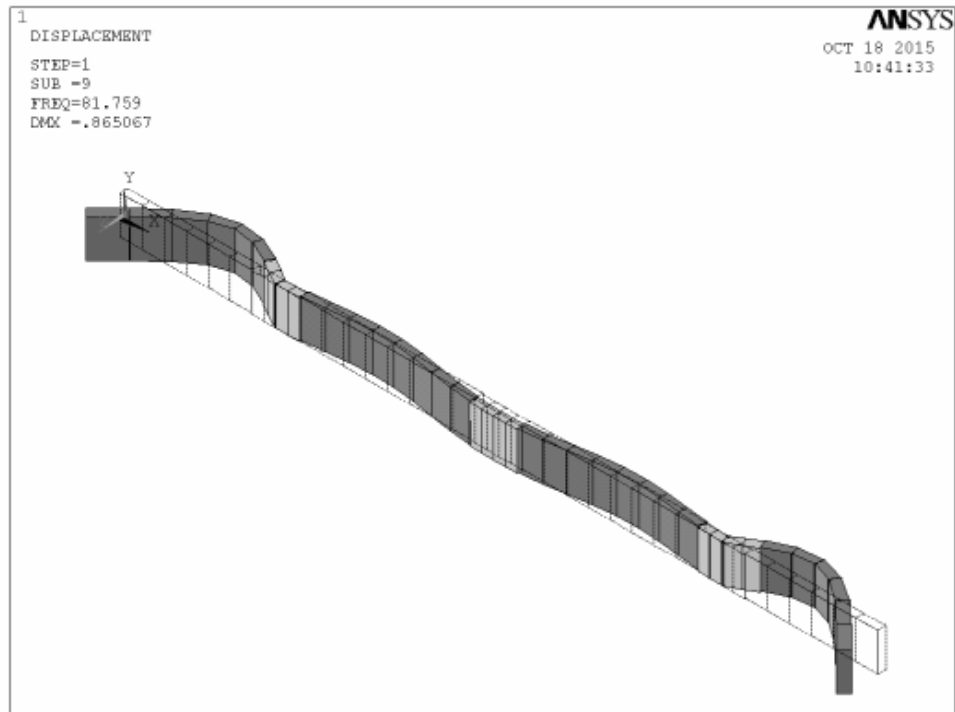


Figure 3.17. Flapping 6



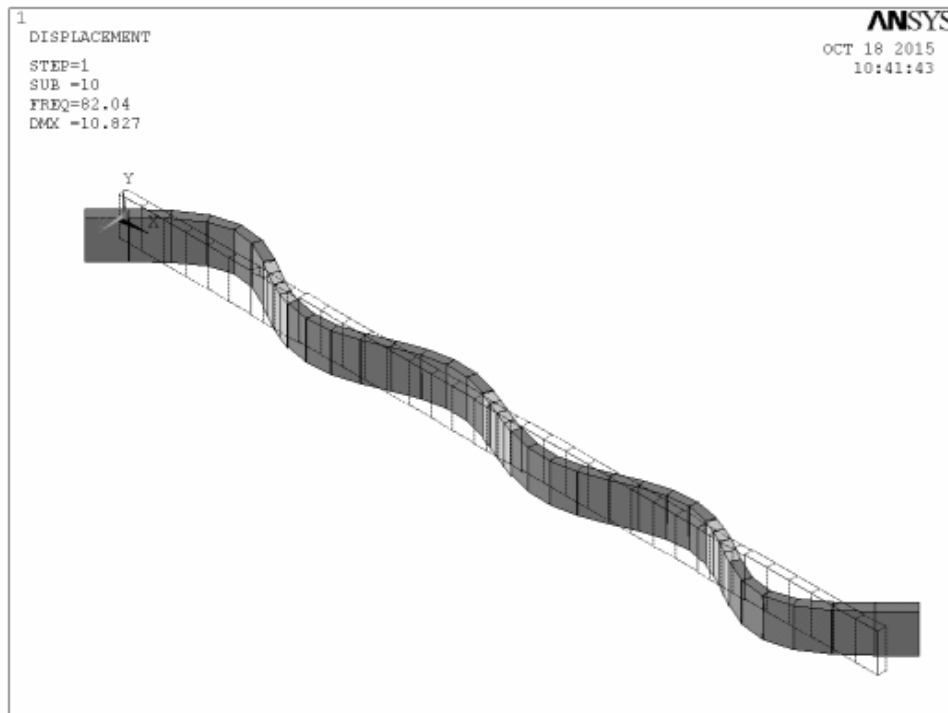


Figure 3.18. Flapping 7

### 3.5. Natural Frequencies and Mode Shapes of Several Models

In order to see the effects of the ratio of span to length  $\alpha = S/L$  on the natural frequencies, considering the same lengths of the thickened cross-section part  $L2$  and of total length  $=2L1+3L2+2L3$  shown in Figure 3.8, the models with different  $L1$  and  $L3$  combinations are studied. Each model is named based on the notation  $Model_{L1}$  as follows:

$Model_{2200}$  :  $L1 = 2200$  mm,  $L2 = 500$  mm and  $L3 = 1050$  mm.

$Model_{2000}$  :  $L1 = 2000$  mm,  $L2 = 500$  mm and  $L3 = 1250$  mm.

$Model_{1800}$  :  $L1 = 1800$  mm,  $L2 = 500$  mm and  $L3 = 1450$  mm.

$Model_{1600}$  :  $L1 = 1600$  mm,  $L2 = 500$  mm and  $L3 = 1650$  mm.

$Model_{1400}$  :  $L1 = 1400$  mm,  $L2 = 500$  mm and  $L3 = 1850$  mm.

$Model_{1200}$  :  $L1 = 1200$  mm,  $L2 = 500$  mm and  $L3 = 2050$  mm.

$Model_{1000}$  :  $L1 = 1000$  mm,  $L2 = 500$  mm and  $L3 = 2250$  mm.

In addition to investigation of effect of the ratio of span to length  $\alpha = S/L$  on the natural frequencies, next to that, by using the same ratio of span to length denoted by  $\alpha = S/L=4700/8000=0.5875$ , different  $L1$ ,  $L2$ , and  $L3$  combinations are considered in order to see the effects of the thickened cross-section part on the natural frequencies. Similar to former study step, now each model is named based on the notation  $\text{Model}_{L2}$  as follows:

$\text{Model}_{300}$  :  $L1 = 1500$  mm,  $L2 = 300$  mm and  $L3 = 2050$  mm.

$\text{Model}_{400}$  :  $L1 = 1450$  mm,  $L2 = 400$  mm and  $L3 = 1950$  mm.

$\text{Model}_{500}$  :  $L1 = 1400$  mm,  $L2 = 500$  mm and  $L3 = 1850$  mm.

$\text{Model}_{600}$  :  $L1 = 1350$  mm,  $L2 = 600$  mm and  $L3 = 1750$  mm.

$\text{Model}_{700}$  :  $L1 = 1300$  mm,  $L2 = 700$  mm and  $L3 = 1650$  mm.

It should be noted for  $\text{Model}_{2200}$  and  $\text{Model}_{300}$  that if the subscript of the model name has 4 digits, it belongs to  $L1$ , otherwise it belongs to  $L2$ .

The results of the analysis on investigation on the effect of the ratio of span to length  $\alpha = S/L$  on the natural frequencies are presented for ten natural frequencies in Figure 3.19 to Figure 3.28 separately, in order to see the graph precisely. The axis of the plots in the aforementioned figures are selected as  $L1$  (mm) vs  $n^{\text{th}}$  (Hz) frequency. Moreover, in the plots gridlines are shown to see the numerical value for a selected point to discuss.

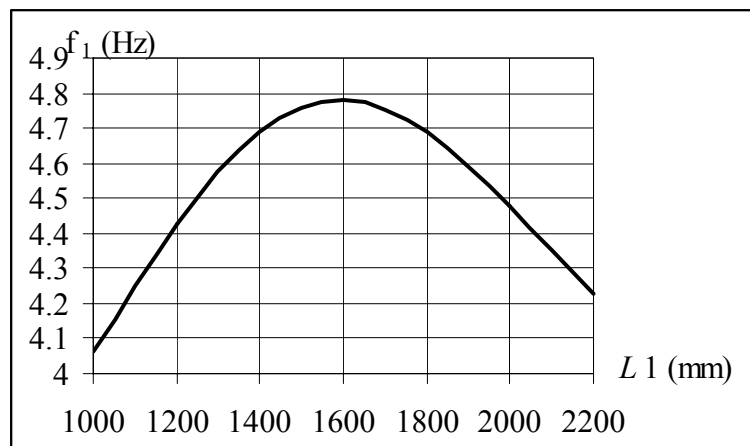


Figure 3.19. The effect of  $L1$  on first natural frequencies

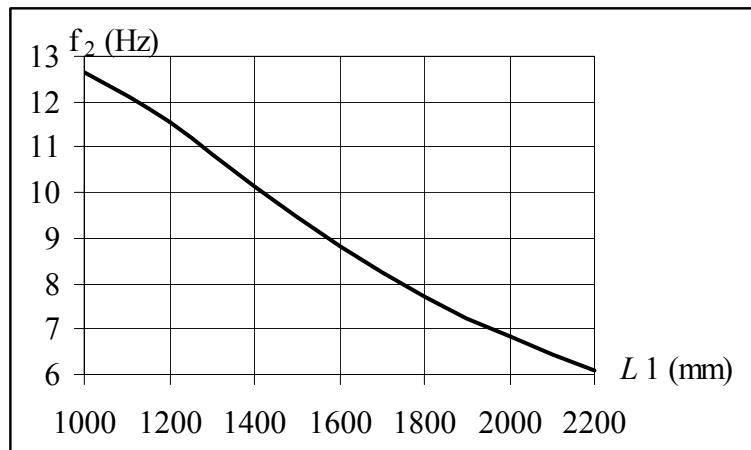


Figure 3.20. The effect of  $L_1$  on second natural frequencies

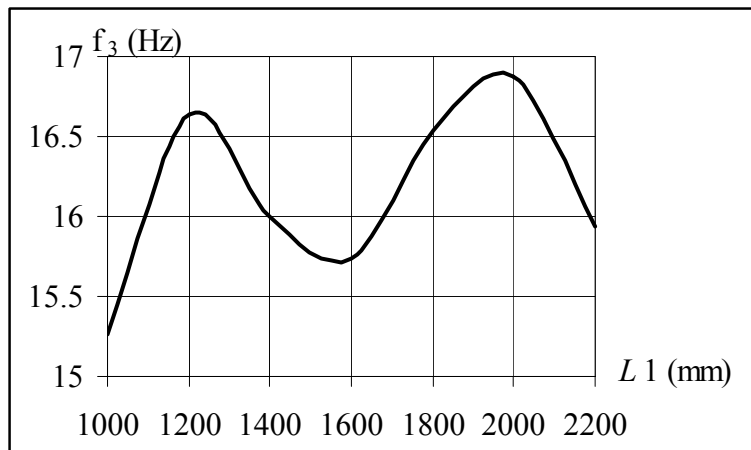


Figure 3.21. The effect of  $L_1$  on third natural frequencies

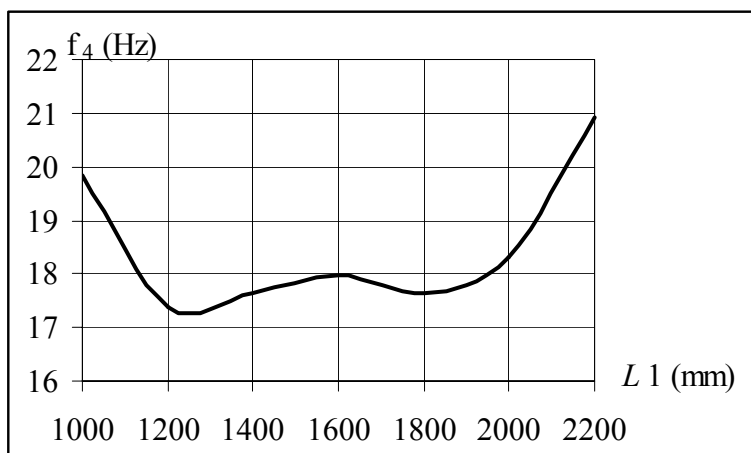


Figure 3.22. The effect of  $L_1$  on fourth natural frequencies

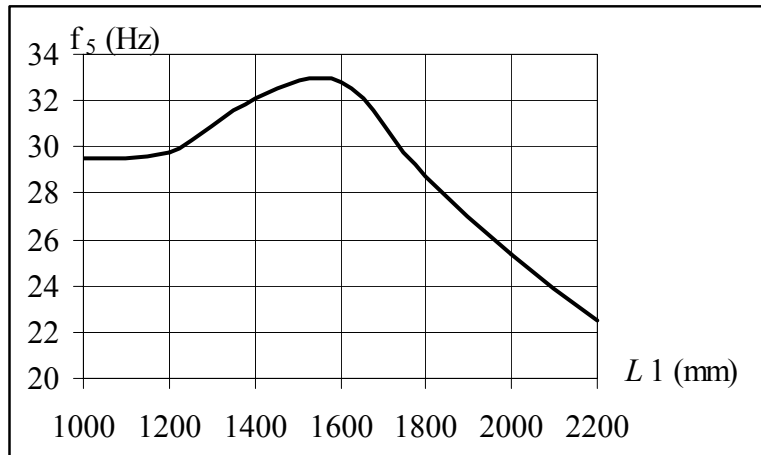


Figure 3.23. The effect of  $L_1$  on fifth natural frequencies

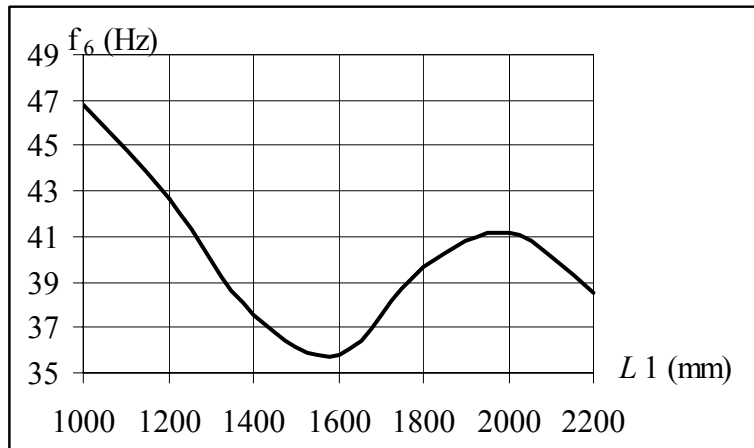


Figure 3.24. The effect of  $L_1$  on sixth natural frequencies

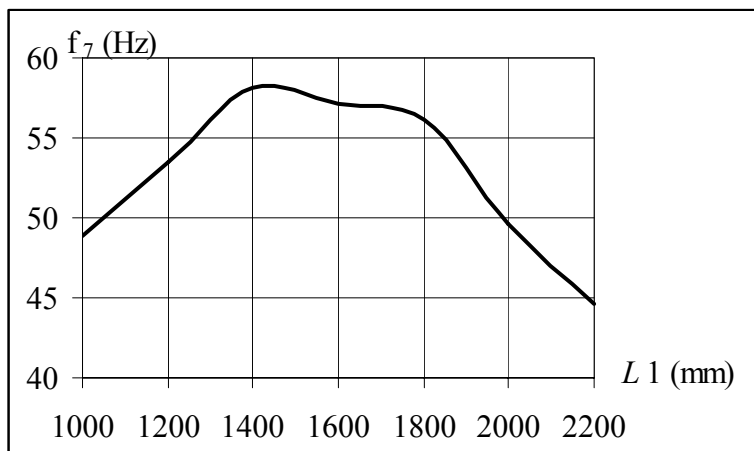


Figure 3.25. The effect of  $L_1$  on seventh natural frequencies

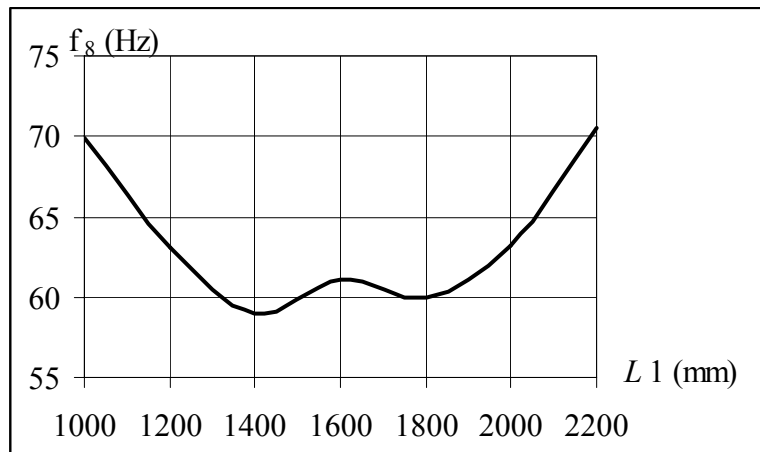


Figure 3.26. The effect of  $L_1$  on eighth natural frequencies

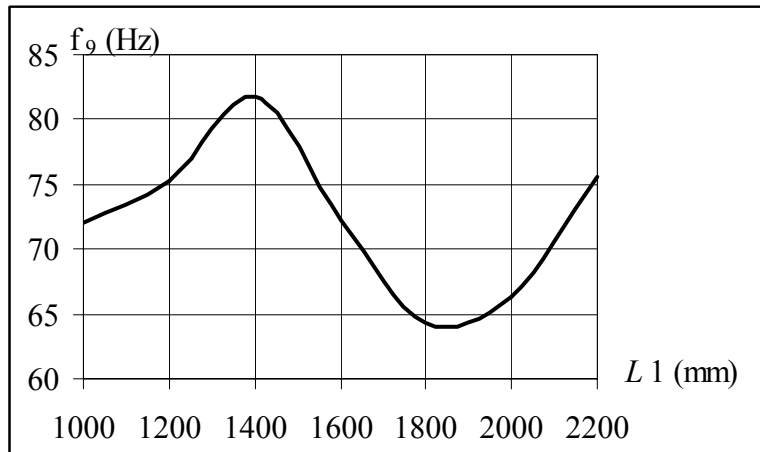


Figure 3.27. The effect of  $L_1$  on ninth natural frequencies

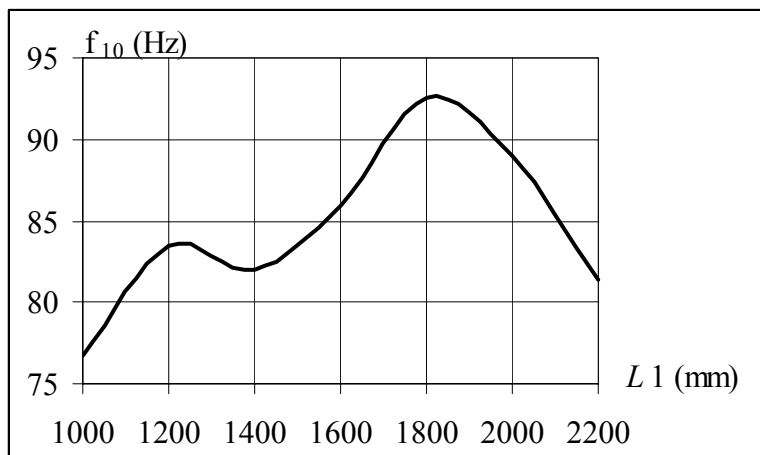


Figure 3.28. The effect of  $L_1$  on tenth natural frequencies

Since the overhang length  $L1$  is effective on the location of nodes of natural modes, the results related to in the range of  $\{1000, \dots, 2200\}$  shown in Figure 3.19 to Figure 3.28 have very different plots. Discussions of them are presented below:

First natural frequencies has maximum value for  $L1=1600$  mm and the plot in the shape of inverse parabola.

Second natural frequency decreases about linearly, when the overhang length  $L1$  increases.

Third natural frequency plot in the shape of fourth order polynomial. It has local maximum at  $L1=1200$  mm, local minimum at  $L1=1600$  mm, and absolute maximum at  $L1=2000$  mm.

Fourth natural frequency plot in the shape of inverse fourth order polynomial. It has absolute minimum at  $L1=1200$  mm, local maximum at  $L1=1600$  mm, and local minimum at  $L1=2000$  mm.

Fifth natural frequencies increase up to  $L1=1550$  mm gradually, then decrease linearly.

Sixth natural frequencies decrease up to  $L1=1400$  mm, then increase until local maximum value at  $L2=2000$  mm, finally again decrease linearly.

Seventh natural frequency has maximum value for  $L1=1400$  mm and the plot approximately in the shape of inverse parabola.

Eighth natural frequency plot in the shape of inverse fourth order polynomial. It has absolute minimum at  $L1=1400$  mm, local maximum at  $L1=1600$  mm, and local minimum at  $L1=1800$  mm.

Ninth natural frequencies increase up to  $L1=1400$  mm, then decrease until local minimum value at  $L2=1850$  mm, finally again increase linearly.

Tenth natural frequency plot in the shape of fourth order polynomial. It has local maximum at  $L1=1200$  mm, local minimum at  $L1=1400$  mm, and absolute maximum at  $L1=1800$  mm.

The results of the analysis on investigation of the effects of the thickened cross-section part length  $L2$  on the natural frequencies are presented just for three natural frequencies in Figure 3.29 to Figure 3.31 separately, in order to see the graph precisely. The axis of the plots in the aforementioned figures are selected as  $L2$  (mm) vs  $n^{\text{th}}$  (Hz) frequency. Moreover, in the plots gridlines are shown to see the numerical value for a selected point to discuss.

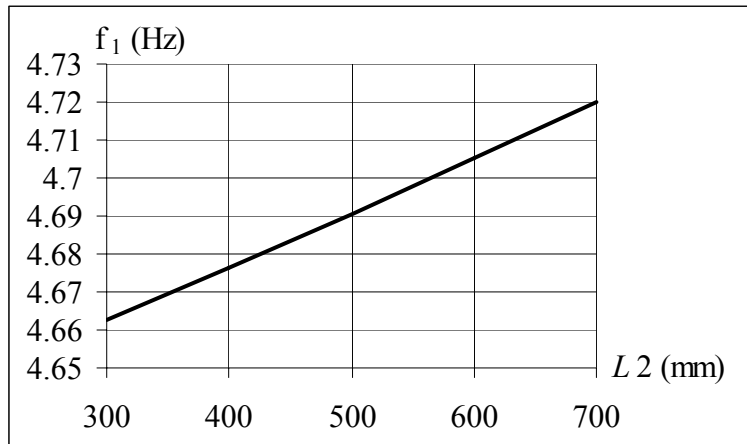


Figure 3.29. The effect of  $L_2$  on first natural frequencies

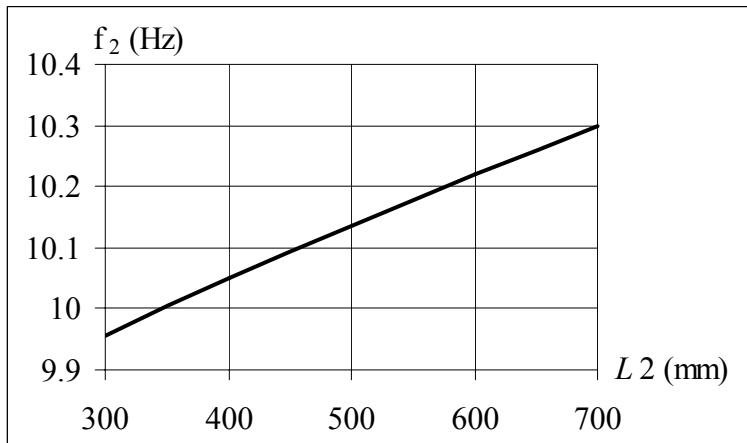


Figure 3.30. The effect of  $L_2$  on second natural frequencies

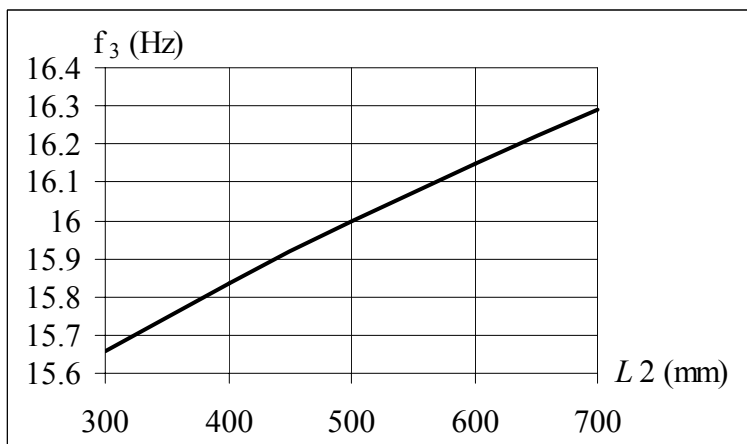


Figure 3.31. The effect of  $L_2$  on third natural frequencies

It can be seen from Figure 3.29 to Figure 3.31 that when the thickened cross-section part length  $L_2$  increases in the considered range, natural frequencies increases linearly. Although the same tendency is observed for the first ten natural frequencies, just first three natural frequency results are presented.



## CHAPTER 4

### CONCLUSIONS

Modal analysis of aerofoil cross-sectioned wing made of laminated composite and filled with foam can be studied by Finite Element Method with the help of ANSYS. ANSYS provides different types of finite element models based on beam and shell elements. The effects of ratio of overhangs to mid-span and length of the thickened parts on natural frequencies are investigated by finite element models developed in ANSYS and the model is verified by theoretical results available in the literature.

Since the overhang length  $L1$  is effective on the location of nodes of natural modes, very different type of plots for natural frequency vs length  $L1$  are obtained.

Moreover, length of the thickened cross-section part  $L2$  and the natural frequencies are directly proportional.

## REFERENCES

- Blasques JP, Stolpe M. 2012 Multi-material topology optimization of laminated composite beam cross sections. *Composite Structures*; 94(11):3278–3289.
- Euler L., 1744. *De curvis elasticis*, Lausanne and Geneva: Bousquet.
- Hodges D.H., Atilgan A.R., Fulton M.V., Rehfield L.W. 1991. Free-vibration analysis of composite beams, *Journal of American Helicopter Society* 36(3): 36–47.
- Inman, D.J. 2001 *Engineering Vibration*, Second edition, New Jersey, Prentice-Hall.
- Jang, S.K. and Bert, C.W. 1989 Free vibration of stepped beams: exact and numerical solutions. *Journal of Sound and Vibration* 130: 342–346.
- Kaw, A.K. 2006. *Mechanics of composite materials*. Boca Raton, CRC Press.
- Murphy, J.F. 1997. Transverse vibration of a simply supported beam with symmetric overhang of arbitrary length. *Journal of Testing and Evaluation*. 25: 522–524.
- Murugan, S., Ganguli, R. and Harursampath, D. 2012 “Surrogate based design optimisation of composite aerofoil cross-section for helicopter vibration reduction”, *The Aeronautical Journal*,. 116: No: 1181, 2012.
- Meirovitch, L. 1967. *Analytical methods in vibrations*. New York: Macmillan Publishing Co.
- Marur S. and Kant T. 1996 Free vibration analysis of fiber reinforced composite beams using higher order theories and finite element modelling, *Journal of Sound and Vibration* 194: 337–351.
- Qatu, M.S. 2004. *Vibration of Laminated Shells and Plates*, Netherlands: Elsevier Ltd.
- Reddy, J. N. 1992 *Finite Element Analysis of Composite Laminates* London: Kluwer Academic Publishers
- Schubel, P.J. and Crossley, R.J. 2012. Wind turbine blade design, *Energies*: 5: 3425-3449.
- Singa-Rao, K. and Amba-Rao, C.L. 1973, Vibration of Beams with Overhangs, *AIAA Journal* 11: 1445-1446.
- Spera, D.A. 2009. *Wind Turbine Technology: Fundamental Concepts of Wind Turbine Engineering*, New York: ASME Press.

- Stafford, R.O. and Giurgiutiu, V. 1975. Semi-analytic methods for rotating Timoshenko beams, *International Journal of Mechanical Science* 17: 719-727.
- Subic, A. and He, J. 1995, A case study on modal analysis of a glider wing, 13th International modal analysis conference, 1694-1700.
- Subramanian P. 2006. Dynamic analysis of laminated composite beams using higher order theories and finite elements, *Composite Structures* 73: 342–353.
- Tenguria, N.; Mittal, N. D.; and Ahmed, S. 2010. Design and Finite Element Analysis of Horizontal Axis Wind Turbine blade. *International Journal of Applied Engineering Research* 1: 500-507.
- Tenguria, N.; Mittal, N. D.; and Ahmed, S. 2011. Modal Analysis for Blade of Horizontal Axis Wind Turbine, *Asian Journal of Scientific Research* 4: 326-334.
- Timoshenko S.P. 1922. On the transverse vibrations of bars of uniform cross section. *Philosophical Magazine*: 43 125-131.
- Tsai, S.W. 1980, Introduction to composite materials. Lancaster-Pennsylvania, Technomic Publishing Company.
- Yanbin C., Lei, S. and Feng, Z. 2010, Modal analysis of wind turbine blade made of composite laminated plates, Power and Energy Engineering Conference (APPEEC).
- Yardimoglu, Bulent 2012. Lecture Notes on Advance Vibrations, Izmir: Izmir Institute of Technology.
- Yu, M.C. and Hwu, Chyanbin, 2005. Free Vibration Analysis of Tapered Composite Wings, Advanced Materials Development & Performance Conference, Auckland, NewZealand 166